EFFECT OF SIDE CHAIN LENGTH AND STIFFNESS ON THE ADSORPTION OF METHACRYLATE BASED POLYMERS

by

Emre KIRGIN

B.S., Chemistry, Yildiz Technical University, 2016

Submitted to the Institute for Graduate Studies in
Science and Engineering in partial fulfillment of
the requirements for the degree of
Master of Science

Graduate Program in Chemistry

Boğaziçi University

2020

ACKNOWLEDGEMENTS

Firstly, I would like to thank my supervisor Assoc. Prof. Bülent Akgün for giving me the opportunity to work in his laboratory and for his guidance. He always supported me to follow my scientific curiosity throughout my master project. I am also thankful to my thesis committee members Assoc. Prof. Oktay Demircan, Prof. Duygu Avcı Semiz and Assoc. Prof. Uğur Ünal for spending their valuable time to evaluate my thesis.

I am grateful to members of our laboratory; Sümeyye Özer, Ayşe Çağlayan and Çağatay Yılmazoğlu for their help during my experiments and their friendship outside the laboratory.

I want to thank specially Bora Garipcan for his friendship and support during my master studies and writing the thesis. Along with him, I also want to thank specially Aybüke Garipcan, Beren Aylan, Mesut Berber, Can Gürkaşlar, Kübra Zırhlıoğlu and Orhun Külekçi for their friendship and motivating me during difficult times.

Additionally, I would like to thank my gamer friends Akif Akçelik and Evren Demirkıran for helping me push real-life problems with the virtual world and for their friendship.

I would like to thank Boğaziçi University and TÜBİTAK for their financial support during my master thesis.

Finally, I am grateful to my parents Hatice and Mehmet Kırgın, my sister Dilara, for their love and endless support under all circumstances and in every decision that I have taken. My special thanks go to my dream partner Açelya Yılmazer whose love and support enabled me to overcome every difficult step I met during my master study.

ABSTRACT

EFFECT OF SIDE CHAIN LENGTH AND STIFFNESS ON THE ADSORPTION OF METHACRYLATE BASED POLYMERS

Polymer thin films provide a multifunctional platform to alter the physical, chemical, and biological properties of a wide variety of substrates. To remove residual stresses and solvents, they are annealed above their glass transition temperature (T_g). Polymer chains are adsorbed to the substrate during annealing and presence of the adsorbed layer causes deviation in physical properties. Earlier work elucidated the kinetics of adsorption, structure of the adsorbed layers, as well as the effect of these layers on the physical properties for the linear polymer chains, the effect of the side chain length and stiffness on the adsorption remained completely unknown. Herein, we have investigated adsorption behavior of methacrylate-based polymers with different side chain length and stiffness on hydrophobic passivated silicon (Si-H) and hydrophilic SiO_x surfaces. Thickness and growth kinetics of adsorbed layers are determined using ellipsometry, layer structure is resolved by X-ray reflectivity (XR), and the extent of the competing side reactions are monitored using attenuated total reflectance-infrared spectroscopy (ATR-IR). Increasing side chain length decreased the thickness of the adsorbed layers on both surfaces relative to PMMA. Bulky tertiary butyl groups caused an increase in the thickness of the adsorbed layer on SiH surface but has no impact on the SiO_x surface. Introduction of neopentyl group yield the thickest adsorbed layer on SiH surface and restore the strength of segment–substrate interactions on SiO_x surface. Isobornyl group, the stiffest side group used in this work, provided the thickest adsorbed layer on SiO_x surface. Adsorbed layers on SiH surfaces are represented quite well with single layer model whereas on SiO_x a bilayer model was necessary to fit the data. Thermal decomposition reactions at high temperatures compete with the adsorption process and robust crosslinked layers were obtained under these circumstances.

ÖZET

METAKRİLAT BAZLI POLİMERLERDE YAN ZİNCİR UZUNLUĞU VE SERTLİĞİNİN ADSORPSİYONA OLAN ETKİSİ

Polimer ince filmler, çeşitli substratların fiziksel, kimyasal ve biyolojik özelliklerini değiştirmek için çok işlevli bir platform sağlar. Artakalan gerilmeleri ve çözücüleri uzaklaştırmak için camsı geçiş sıcaklıklarının (T_g) üzerinde tavlanırlar. Polimer zincirleri tavlama sırasında substrata adsorbe olur ve adsorbe tabakanın varlığı fiziksel özelliklerde sapmaya neden olur. Daha önceki çalışmalar adsorpsiyon kinetiğini, adsorbe edilmiş tabakaların yapısını ve bu tabakaların lineer polimer zincirleri için fiziksel özellikler üzerindeki etkisini açıklasa da, yan zincir uzunluğunun ve sertliğinin adsorpsiyon üzerindeki etkisi tamamen bilinmemektedir. Burada hidrofobik pasifleştirilmiş silikon (Si-H) ve hidrofilik SiO_x yüzeylerinde farklı yan zincir uzunluğu ve sertliğine sahip metakrilat esaslı polimerlerin adsorpsiyon davranışını inceledik. Adsorbe tabakaların kalınlığı ve büyüme kinetiği elipsometri kullanılarak belirlendi, tabaka yapısı X-ışını yansıtma (XR) ile aydınlatıldı ve rakip yan reaksiyonların derecesi zayıflatılmış toplam yansıma-kızılötesi spektroskopisi (ATR-IR) kullanılarak izlendi. Yan zincir uzunluğunun arttırılması, PMMA'ya göre her iki yüzeydeki adsorbe tabakaların kalınlığını azalttı. Hacimli üçüncül butil grupları, adsorbe tabakanın SiH yüzeyi üzerindeki kalınlığında bir artışa neden oldu, ancak SiO_x yüzeyi üzerinde hiçbir etkisi yoktur. Neopentil grubunun eklenmesi, SiH yüzeyinde en kalın adsorbe edilmiş katmanı verdi ve SiO_x yüzeyinde segment-substrat etkileşimlerinin gücünü geri kazandırdı. Bu çalışmada kullanılan en sert yan grup olan izobornil grubu, SiO_x yüzeyindeki en kalın adsorbe tabakayı sağlamıştır. SiH yüzeylerindeki adsorbe tabakalar, tek katmanlı model ile oldukça iyi temsil edilirken SiO_x'de verilere uyacak şekilde iki katmanlı bir model gerekliydi. Yüksek sıcaklıklarda termal bozunma reaksiyonları adsorpsiyon prosesi ile rekabet etmiştir ve bu koşullar altında sağlam çapraz bağlı katmanlar elde edildi.

TABLE OF CONTENTS

LIST OF FIGURES

LIST OF TABLES

LIST OF SYMBOLS

cm	Centimeter
h	Hour
k_B	Boltzmann Constant
kV	Kilovolt
mA	Miliampere
ml	Mililiter
nm	Nanometer
T	Temperature
μm	Micrometer
Å	Angstrom
^oC	Degree Celcius
θ	Theta
β	Beta

LIST OF ACRONYMS/ABBREVIATIONS

ATR-FTIR	Attenuated Total Reflectance - Fourier Transform Infrared
HF	Hydrofluoric Acid
HPLC	High Performance Liquid Chromatography
H_2O_2	Hydrogen Peroxide
H_2SO_4	Sulfuric Acid
M_n	Number Avarage Molecular Weight
$NaHCO_3$	Sodium Bicarbonate
PDI	Poly Dispersity Index
PMA	Poly(Methacrylic Acid)
PMMA	Poly(Methly Methacrylate)
PnBMA	Poly(n-Butyl Methacrylate)
PnHMA	Poly(n-Hexyl Methacrylate)
a-PtBMA	Atactic Poly(tert-Butyl Methacrylate)
i-PtBMA	Isotactic Poly(tert-Butyl Metharcylate)
PneoPMA	Poly(neo-Pentyl Methacrylate)
PiBoMA	Poly(isobornyl Methacrylate)
PGA	Poly(Glutaric Anhydride)
PVAc	Poly(Vinyl Acetate)
rpm	Revolutions Per Minute
SiH	Passivated Silicon
SiO_x	Silicon Oxide
SLD	Scattering Length Density
T_g	Glass Transition Temperature
UV	Ultraviolet
XPS	X-ray Photoelectron Spectroscopy
XRR	X-ray Reflectivity

1. INTRODUCTION

1.1. Polymer Thin Films

Polymer thin films offer a multifunctional platform for adjusting the physical, chemical, and biological properties of a wide range of substrates to create antifouling metarials, biosensors, light-emitting diodes, organic photovoltaic devices, high charge density batteries, functional membranes, lithographic coatings, corrosion resistance layers, colloid stabilization, and controlled release scaffolds [1] [2] [3]. In these applications, polymer coatings can make a substrate biocompatible, enhance a material's thermal, mechanical, or chemical stability, increase wear protection, durability or lifetime, diminish friction or inhibit corrosion. That being said, the performance of polymer thin films highly depends on the synthesis, deposition techniques, polymer composition, annealing conditions and the surface properties [4].

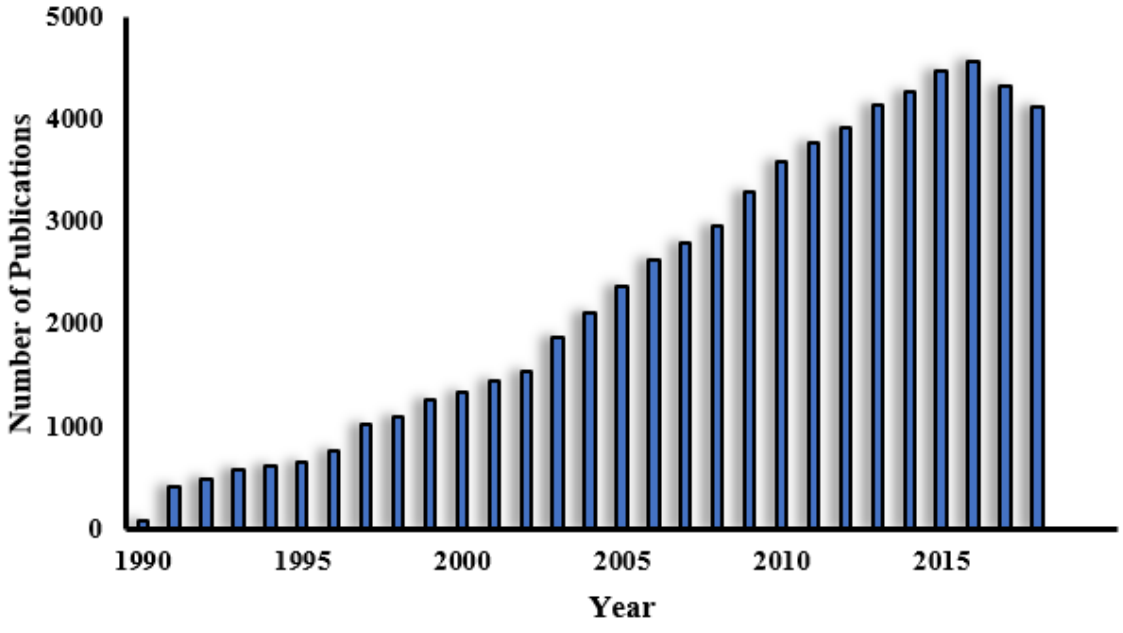

Figure 1.1. Number of publications with the keyword "polymer thin film" (Source: Web of Science, data retrieved on 2019).

Over the last 30 years, an immense amount of experimental and computational studies on polymer thin films has been carried out and the number of publications about polymer thin films has increased each year (Figure 1.1). Since 2017, the number of publications seems to decrease, however this is due to different keywords are used for new hot areas such as nanocomposites. These are still polymer thin films coated on nanoparticles but the polymer thin film keyword is rarely used in these publications.

1.2. Polymer Adsorption

Thin polymer films are always annealed above their glass transition temperature, T_g, before they are used in applications to remove residual stress and solvents remained from deposition processes. Adsorption of polymer chains occur during the annealing process. Polymer chains tend to form adsorbed layers on non-repulsive surfaces even with monomer-substrate interaction strength less than k_BT via physisorption [5]. These interactions could be hydrogen bonding, Van der Waals forces or hydrophobic interactions. Even though each monomer may be pinned to the substrate with energy of kT or less, since there are multiple segments pinning at the same time, the total interaction energy could be a few tens to thousands of kT. Total interaction energy depends on the molecular weight [5].These interactions are dynamic in origin. Some of them desorb from the surface when others are adsorbing. Due to very low probability of desorbing all the monomers at the same time, whole chain desorption is not likely and these chains are assumed to be irreversibly adsorbed within the timescales of months and years. If the interaction energy is two or more orders of magnitudes higher than k_BT it is considered as chemisorption [6]. In chemisorption, covalent bonds occur between substrate and the polymer chain, thus it is also irreversible. Earlier theoretical work considered the adsorption from solution and they assumed no interaction between adsorbed polymer chains. Later Silberberg [7] and Hoeve [8] taken polymer-polymer interactions into account, however they did not consider the contribution of tails due to segment density profile they have chosen. Later, Schuetjens and Fleer [9] able to calculate number of chains in train, loop and tail conformations in equilibrium using quasi-crystalline lattice model. These adsorbed chain conformations are shown

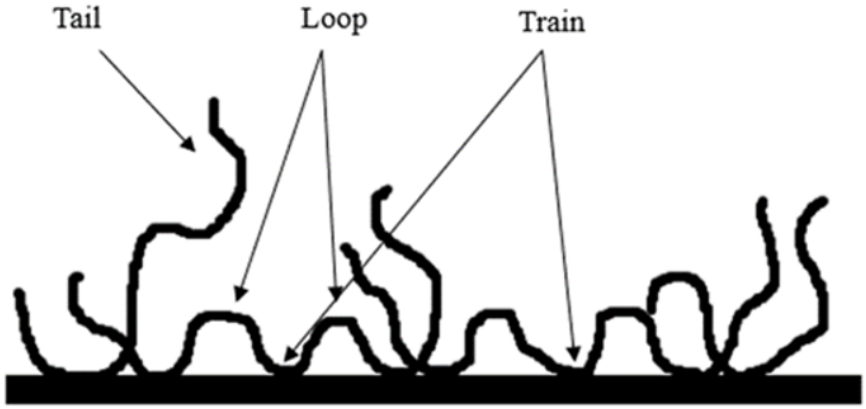

Figure 1.2. Tail, loop and train conformation of adsorbed polymer chains.

in Figure 1.2. Trains have multiple segmental contact points at the substrate, the non-adsorbed segments between the pinned segments are called as loops, and tails are the free ends of the chains that are adsorbed loosely to the substrate [10].

1.2.1. Thermodynamic of Polymer Adsorption

Polymer adsorption is driven by the balance between two parameters, enthalpic gain due to segment-substrate interactions and conformational entropy loss (Figure 1.3). Polymer chains adsorb to the substrate if there are even weakly attractive forces between the polymer and the substrate. Total energy gained through segment-substrate interactions is additive. Therefore, the number of contacts is a crucial parameter. Linear polymers make $N^{1/2}$ contacts with the underlying substrate, therefore enthalpic gain becomes larger as the molecular weight of the polymer increases. However, as polymer chains are pinned to the substrate, they are not able to search all three dimensional space and their conformational entropies decrease significantly. The balance between the enthalpic gain and entropic loss dictate the equilibrium structure of the adsorbed layer. To reach equilibrium state, polymer thin films annealed above their glass transition temperature (T_g) for extended period of time and leached several time

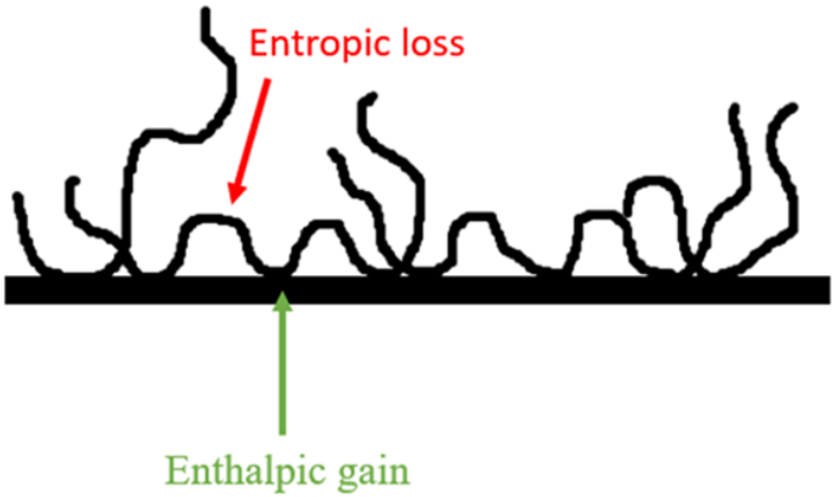

Figure 1.3. Thermodynamic of polymer adsorption.

with good solvent to remove non-absorbed polymer chains [11] [12].

Gin et al. [13] investigated the adsorption of polystyrene (PS) chains from melt using initially 50 nm thick spun-cast PS layers by X-ray reflectivity (XR) and atomic force microscopy (AFM). Fitting XR curves with bilayer model revealed two discrete layers with different mass densities. The layer next to the substrate has a higher density than the PS in bulk and the layer above that has a bulk-like density. They proposed that the bottom layer is composed of early-arriving chains which can make multiple contacts with the substrate to mostly form train conformations. They called this layer as flattened layer. The chains on top of this layer are called as loosely adsorbed chains since when they arrive to the substrate, most of the surface sites are already covered by the polymer segments so they can only make a few contacts and their conformation is dominated by the loops and tails. Thickness of the flattened layer is found to be independent of the molecular weight [12], whereas the thickness of the loosely adsorbed layer is molecular weight dependent [14].

1.3. Effect of Adsorbed Layers on Physical Properties

Adsorbed polymer layers have attracted great interest because their presence within thin films cause deviations in physical properties such as T_g [15], viscosity [16], crystallization time [17], surface fluctuations [18] and diffusion [19].

Viscosity of thin polymer films is a very hard to measure physical property. In general, it is obtained through indirect measurements by measuring either dynamics of polymer chains or surface fluctuations as a function of thickness at different temperatures or following the mobility of probe molecules such as gold nanoparticles within polymer matrix. Koga and coworkers [16] have used the latter approach to measure the viscosity of PS thin films as a function of depth using X-ray photon correlation spectroscopy (XPCS). Gold nanoparticles were submerged in approximately 60 nm thick PS films above bulk T_g of PS. XPCS measurements demonstrated that viscosity at the center of the film is factor of 10 higher than that on the air surface. They explained this big difference observed over 30 nm depth by the existence of adsorbed chains at the substrate interface. They assumed that the mobility of these adsorbed chains significantly hindered due to many segment-substrate interactions. They proposed the gradient in viscosity over 60 nm distance with the limited mobility of PS chains at the substrate is propagated through entanglement of non-adsorbed chains to adsorbed chains.

Correlation between adsorption and crystallization is investigated by Martinez-Tong et al. [17] using dielectric relaxation spectroscopy. They have measured the dielectric loss modulus as a function of time for poly(L-lactide) films of various thicknesses sandwiched between aluminum layers. They have found that the crystallization time become increasingly longer as the films get thinner and they correlated this behavior with confinement effect down to 25 nm. The slope of the crystallization time vs thickness curve changes dramatically below 25 nm and for films less than 10 nm thick crystallization is not observed within the experimental time scale.

The fact that an adsorbed chain makes ($\sim N^{1/2}$) contacts with the solid surface and decreasing viscosity from air surface to substrate insinuates that adsorbed chains are nearly immobile. This idea was supported with the fact that even at temperatures much higher than the bulk T_g of PS, no thermal expansion of adsorbed PS chains [13] and no interdiffusion to adsorbed PS layer [16] were observed. Jiang and coworkers take it one step further and they have studied long-range perturbations in chain mobility associated with the adsorbed layer. They monitored the broadening of interface in bilayer samples of H-PS/D-PS to elucidate diffusive chain dynamics using high-pressure neutron reflectivity (NR). The diffusion dynamics at 0.6 R_g away from the substrate is strongly hindered (factor of 10) and recovered to bulk diffusion when the same interface is 3 R_g or more away from the substrate. They have concluded that in the presence of CO_2, an efficient polymer plasticizer, the entanglements between the adsorbed chains and neighboring non-adsorbed chains remain powerful. These entanglements are responsible for long-range deviations in chain mobility. Formation of loops in the adsorbed chains is very important for the above-mentioned entanglement picture [19].

Many research groups have investigated the glass transition temperature of thin films under confinement and conclusion from their work can be reduced to one sentence which is T_g of the thin polymer films decreases with weak substrate polymer interactions and increases with strong attractive interactions [20]. In addition, attractive interactions between polymer and substrate result in mobility reduction [21] [22]. For example, PS, which is weakly interacting with a silicon substrate, exhibits significant negative deviations in T_g from its bulk value for films thinner than 40 nm T_g due to increased free surface mobility [23]. Conversely, silicon substrates with oxide layer can make hydrogen bonds with PMMA and P2VP films that generate positive deviations in film T_g with reduced thickness [24]. However, the direct correlation between T_g values in thin polymer films and adsorbed polymer chains in these films is demonstrated by Napolitano's group [25]. They have shown that the deviation in T_g is a function of free volume exist in the adsorbed chain layer due to packing frustrations. Once the free volume is removed through extensive annealing then the bulk T_g value is recovered.

T_g values for isotactic PMMA (i-PMMA), syndiotactic PMMA (s-PMMA) and atactic PMMA (a-PMMA) polymer films on silicon and aluminum surfaces have been determined using spectroscopic ellipsometry by Grohens and coworkers [26]. They presented a clear association between the density of polymer-substrate interactions and the polymer's T_g at the interface, depending on the tacticity of PMMA. Owing to large density of segment-substrate interactions, T_g of i-PMMA increases dramatically relative to its bulk value whereas s-PMMA with a lower number of interacting segments at the substrate surface show a decrease in T_g. Measurements by infrared reflection absorption spectroscopy (IRAS) demonstrated that density of the segment-substrate interactions decline with syndiotacticity of the polymer. This study unveils the strong correlation between adsorption of chains and deviation in physical properties.

Surface height fluctuations on polymer melts play important roles in wetting, adhesion, and tribology [27] [28]. Kim et al. determined that hydrodynamic continuum theory (HCT) well describes the dynamics of surface height fluctuations for sufficiently thick linear PS films well above their T_g [29]. Foster et al. studied the relaxation of surface height fluctuations for sufficiently thin melt PS films on SiH surface and on plasma polymerized maleic anhydride (ppMA) coated silicon wafers using XPCS [30]. PS Normalized relaxation times for 4 R_g thick films follow the universal curve obtained from HCT, however, for 3 R_g thick films, surface fluctuations are slower compared to calculated values based on HCT. The difference between the calculated and experimental relaxation times were much larger for the films on SiH surface and the authors explained this discrepancy with the adsorption of PS chains on SiH surface. After leaching both polymer films, adsorbed layer was not found on the ppMA substrate whereas 0.5 R_g thick adsorbed layer were obtained on SiH surface.

1.4. Hydrophobicity in Poly(n-Methacrylates)

The way hydrophobicity can be altered by changing the side chain length is important for this study especially for the interpretation of segment-substrate interactions. Feijen and coworkers [31] studied series of poly(n-alkyl methacrylate) with carbon atoms in alkyl groups changing from 1 to 18. They demonstrated that ad-

vancing contact angles increases from 95 to 116 degrees (Figure 1.5) with increasing alkyl length. Receiving contact angles were in between 75 (n = 6) and 40 degrees (n = 12). They explained this hysteresis with reorganization of polymer side chains or segments at the air surface upon contact with water. Increasing the side chain length of poly(n-alkyl methacrylate)s from n = 6 to n = 12 increases the mobility of polymer segments due to internal plasticization. It allows polymer segments to be reorganized at the interface when in contact with water. An additional increase in the length of the side chain (n = 18) increases the mobility of polymer segments and impedes the reorientation at the interface [31].

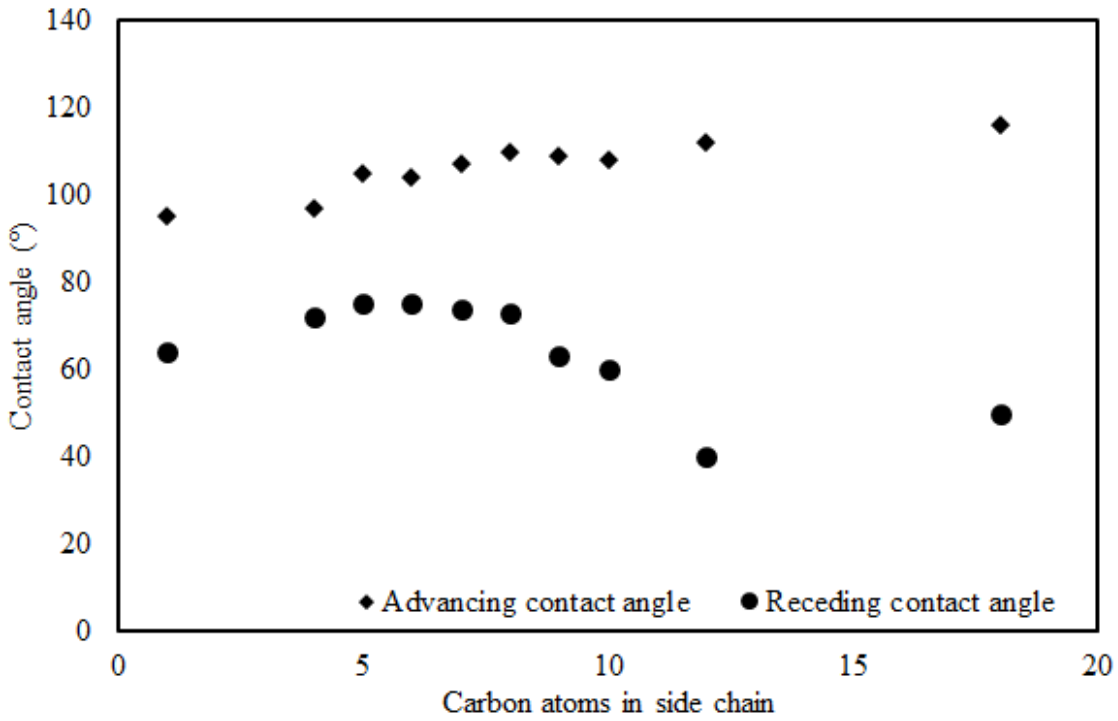

Figure 1.4. Dynamic contact angles of poly(n-alkyl methacrylates) at room temperature.

1.5. Adsorption of Poly(Methyl Methacrylate)

Adsorption of PMMA is studied extensively by a few research groups. Durning et al. [14] investigated formation of adsorbed PMMA layers of different molecular weight on hydroxylated quartz from melt by NR. They prepare polymer films with

concentrated solutions using spin coating that yields 1 μm thickness. When they leached samples without annealing, they observed only 1 nm thick adsorbed PMMA layer independent of molecular weight. However, when they annealed PMMA films, they observed increased adsorbed layer thickness as a function of annealing time and temperature. Adsorbed PMMA layer thickness scaled with molecular weight. Davis et al. [20] looked into homopolymers and random copolymers of styrene and methyl methacrylate in adsorbed layers to eluciadate effect of chemical composition on layer growth and structure with spectroscopic ellipsometry. Using P(S-r-MMA) with different compositions is important in this study, because it allows comparison between van der Waals (for PS) forces and hydrogen bonding (for PMMA) interactions. They proposed that PS chains are adsorbed more loosely because of rather weak interactions with hydrophilic SiO_x substrate. As a result, it forms more tail and loop conformations on surface with respect to PMMA which mainly interacts with the substrate through strong hydrogen bonding and obtain train conformations. They did not find any consistent trend in the layer equilibrium thickness as a function of the composition. However, adsorption mechanism is dominated by either methyl methacrylate or styrene depending on composition. But, nearly equal composition led to huge competition of influences and yield the thinnest adsorbed layer between all the compositions.

Keddie et. al. reported that, T_g of the PMMA film decreases on gold surface and increases on SiO_x surface with decreasing film thickness as a result of hydrogen bonding between PMMA and surface hydroxy groups [21]. Blum and his co-workers [32] studied adsorption of PMMA and poly(vinyl acetate) (PVAc) on silica nanoparticles as well as the impact of adsorption on the T_g of the films. Both polymers have very similar side chain composition but the sequence of functional groups are different. They have measured the T_g difference between adsorbed polymer chains and the same polymer chains in bulk by temperature-modulated differential scanning calorimetry. They found that the T_g normalized with bulk value was always higher for PMMA compared to PVAc indicating PMMA adsorb stronger to silica surface. Molecular simulations revealed that alkoxy oxygen atom of PMMA contributes to the hydrogen bonding due to its shorter distance from the surface compared to alkoxy oxygen in PVAc. This additional hydrogen bonding ability is the reason for increased fraction

of tightly bound chains in adsorbed PMMA layers and therefore suppressed mobility. This study demonstrates that even a small change in the chemical structure of the side chain have significant effects on adsorption behavior and hence on physical properties of the polymer thin films.

2. PURPOSES

Herein, our aim is to investigate systematically the effect of length and stiffness of side chains on the adsorption of methacrylate based polymers Even though adsorption behavior of PMMA on different surfaces have been studied by Durning and Davis [14] [20], adsorption properties of poly(alkyl methacrylates) with respect to increasing side chain length and stiffness are not investigated yet. The results of Mortazavian et al. [32] implied that the small changes in the side chain structure can cause large differences in adsorption behavior and hence physical properties in thin films. We will investigate the adsorption of methacrylate-based polymers with linear side chains of increasing alkyl chain length and with bulky side chains as a function of annealing time at the annealing temperature of T_g + 50 °C. Effect of surface energy of the substrate will be determined by measuring adsorption on hydrophobic passivated silicon (SiH) and hydrophilic silicon oxide (SiO_x) surfaces. It is known that, increasing side chain length in poly(n-alkyl methacrylates) increase hydrophobicity of polymer films [33] [31]. Therefore, one would expect to observe a decrease in the adsorbed layer thickness on SiO_x surface and increase on SiH surface as the side chain length increases. However, we are aware that the hydrophobicity of the polymer chains is not the only parameter that affects the equilibrium layer thickness for adsorbed polymer chains. The growth kinetics and adsorbed layer thickness as a function of annealing time will be monitored using ellipsometry, the layer structure at equilibrium will be determined using X-ray reflectivity (XR), and the chemical structure of the adsorbed layer will be measured by attenuated total reflectance – infrared (ATR-IR) spectroscopy.

3. EXPERIMENTAL

3.1. Materials

Sulfuric acid (H_2SO_4) (98%, Merck), hydrogen peroxide (H_2O_2) (30%, Merck), hydrofluoric acid (HF) (48%, T. J. Baker), toluene (99.7 %, Merck), and sodium bicarbonate ($NaHCO_3$) (99%, Chembio) are used as received. 100 mm diameter and 0.6 mm thick n-type silicon wafers doped with phosphorus are purchased from El-Cat Inc. Silicon wafers are cleaned with piranha solution and UV/Ozone (UV-O_3) treatment to get hydrophilic surface. When hydrophobic surface is desired they are further treated with 2.5 vol. % HF solution to etch the native oxide layer. HF treatment leaves a surface with Si-H groups on top.

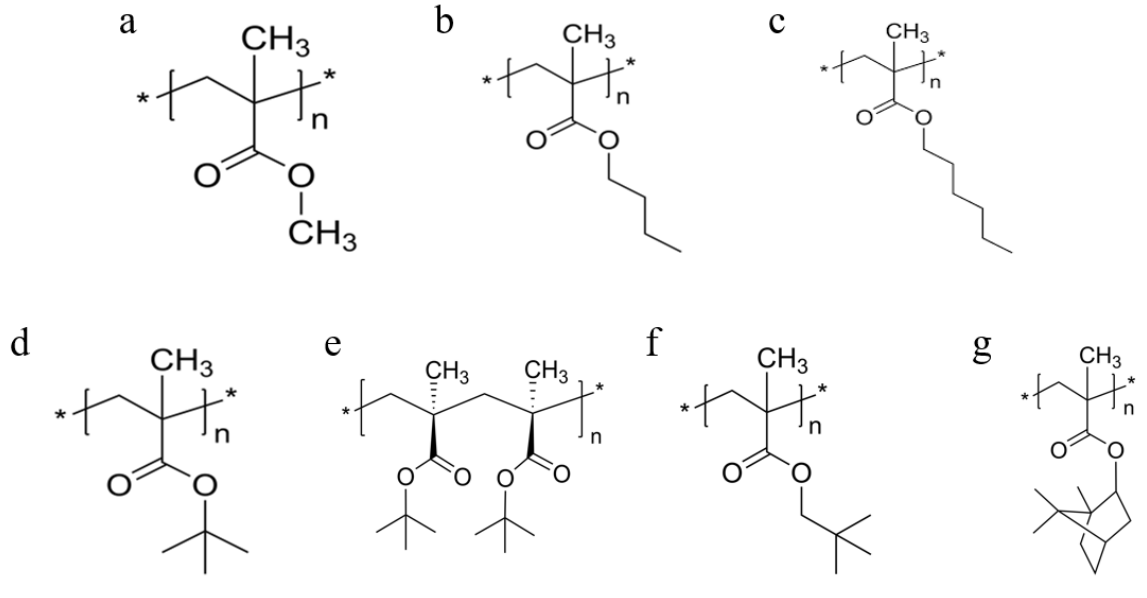

Figure 3.1. Structural representation of methacrylate based polymers used in this study. a) PMMA b) PnBMA c) PnHMA d) a-PtBMA e) i-PtBMA f) PneoPMA g) PiBoMA

Table 3.1: Physical properties of the methacrylate based polymers.

Polymer	**Abbreviation**	**M_N(g)**	**PDI**	**T_g(°C)**
Poly(methyl methacrylate)	PMMA	125000	1.30	130
Poly(n-butyl methacrylate)	PnBMA	128000	1.35	39
Poly(n-hexyl methacrylate)	PnHMA	130000	1.10	-2
Poly(t-butyl methacrylate) (isotactic rich)	i-PtBMA	144500	1.09	9
Poly(t-butyl methacrylate) (atactic rich)	a-PtBMA	125000	1.05	118
Poly(neo-pentyl methacrylate)	PneoPMA	135000	1.05	29
Poly(isobornyl methacrylate)	PiBoMA	130000	1.25	201

Poly (methyl methacrylate) (PMMA) based polymers with different side chain lengths are all purchased from Polymer Source. Names, abbreviations and physical properties of the investigated polymers are given in Table 3.1. Polymers are chosen with number average molecular weights (Mn) between 125 kg/mol and 145 kg/mol and their polydispersities (PDI) range from 1.05 to 1.35. Bulk glass transition temperature (T_g) of each methacrylate based polymer is measured using differential scanning calorimeter (DSC) to determine the annealing temperature for the adsorption measurements.

Polymer solutions in toluene with concentrations varying from 0.25 wt. % to 2 wt. % are prepared to deposit initially 50 nm thick polymer films. Toluene is always freshly filtered using syringe filters that has 45 μm pore size. All the solutions are stirred in toluene for a day to ensure full solubility of all the polymers and provide homogenous solutions.

3.2. Cleaning of Silicon Wafers

Silicon wafers are cleaned first with soap solution, then rinsed with copious amount of distilled water and dried under nitrogen gas. After this pre-cleaning to remove inorganic contaminants, wafers are UV /Ozone (UV/O_3) treated for 30 minutes. Details of the UV/O_3 treatment can be found elsewhere [34]. UV/O_3 treatment removes organic contaminants from the surface and yield a highly hydrophilic surface for adsorption experiments on hydrophobic surfaces.

Fresh piranha solution prepared for each wafer using 35 ml H_2SO_4 and 15 ml H_2O_2. Preparation of piranha solution is an exothermic process and one must be very careful handling it [35]. Silicon wafers are placed in freshly prepared piranha solutions for 30 minutes at 100 ^oC to get rid of organic contamination on the surface. Cleaning of the surface is monitored by the formation of bubbles due to oxidation of organic contaminants to CO_2. After piranha treatment, wafers are washed with distilled water, dried under nitrogen gas, and spin coated right away. For the purpose of alter silicon wafer surface to hydrophobic, silicon wafers are further treated with 2.5 vol. % HF solution. HF solution is prepared by adding 4 ml HF into 80 ml of distilled water. The wafer is placed in the HF solution for 30 seconds and then quickly passed through a crystallizing dish filled with distilled water. Since oxide layer regrows rapidly when the wafer s exposed to air, polymer solutions are spun cast onto treated wafers within 30 seconds.

As soon as the cleaning step of silicon wafers are finalized, wafers are coated with polymer solutions using spin coater at 2200 revolution per minute (rpm). Thickness of the polymer films are measured by ellipsometry and initial thickness of the films are adjusted (using) based on a thickness vs concentration calibration curve.

3.3. Adsorbed Layer Preparation

All the methacrylate based polymers are dissolved in toluene which is a good solvent for them [36]. Once polymers have been fully dissolved, solutions are filtered using

syringe filters of 0,22 μm or 0,45 μm to eliminate any particles. Piranha or HF-cleaned silicon wafers are placed in the spin coater and kept steady by vacuum. Depending on the target film thickness, solutions are dropped onto the wafers using glass pipette and spun cast for a minute between 2000 revolution per minute (rpm) and 3000 rpm. Spin coating is a well-known technique for depositing uniform thin layers of polymer to solid substrates where Newtonian fluid rotates at constant angular velocity. Due to viscous force and surface tension, rapid evaporation of volatile solvent leaves a polymer layer onto the flat surface [37]. Thickness of thin polymer films can be controlled by speed of rotation, rate of evaporation and concentration of the solution. Meyerhofer's equation (Eq. 3.1) [38] indicated that an increase in the solution's viscosity (or concentration) resulted in an increase in the thickness of the layer while an increase in rotational speed caused a decrease in thickness.

$$\frac{dh}{dt} = -\frac{2\rho\omega^2 h^3}{3\eta} - E \tag{3.1}$$

Here, ω is angular velocity, ρ is mass density, η is viscosity, h is fluid layer thickness (not dry) and E is evaporation rate. In this study, rotation time is kept constant for 60 seconds, the concentration of the solution varies according to the desired initial film thickness. Using four different concentration values, solution concentration versus film thickness plot is established at a fixed rotation speed for each polymer, and then film thickness is controlled based on the concentration. Polymer thin films are annealed under vacuum at a temperature above their glass transition, between 1 hour and 192 hours after spin coating. In general, a long annealing process above the T_g of the polymer ensures complete chain relaxation and eliminates residual stress and remaining solvent from the deposition process. Annealing is used here to facilitate the adsorption of polymer chains to the substrate. Once the annealing is complete, samples are removed from the oven and quenched very rapidly at room temperature on an aluminum plate. Samples are then held in toluene for 10 minutes, and the leaching cycle is repeated 5 times in each phase with fresh toluene followed by nitrogen

drying. During leaching, non-adsorbed chains are removed from the substrate so that the samples contain only adsorbed polymer chains.

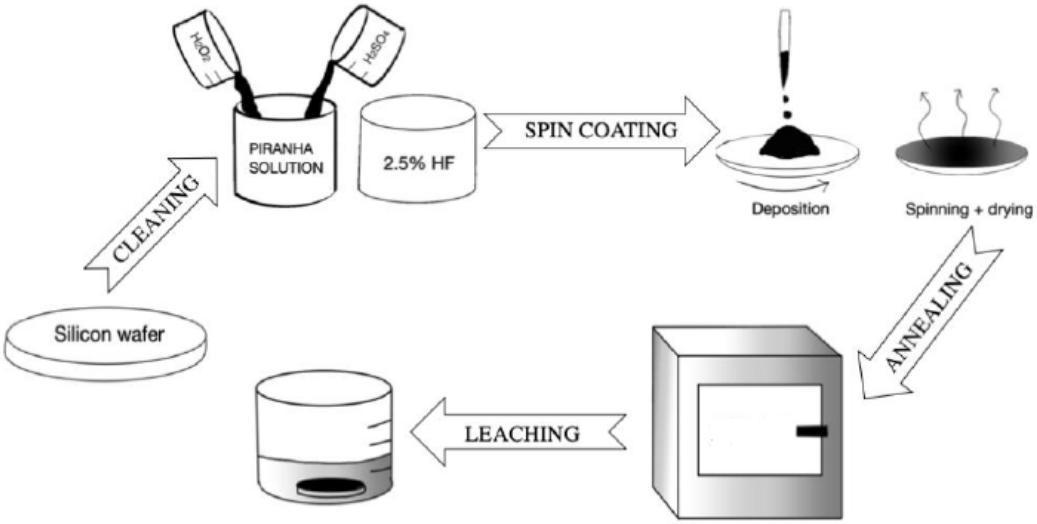

Figure 3.2. Schematic illustration of experimental procedure for adsorbed layer preparation.

3.4. Equipments

The equipments used in this study was listed in Table 3.2 together with their manufactures.

Table 3.2: Equipments.

Vacuum drying oven	Binder, VD23 23L, USA
Analytical Balance	Sartorius, Entris, Germany
Ellipsometry	Film Sense, Multi-Wavelength, USA
X-ray Diffractometer	Bruker, D8 Advance, USA
Heat Block	VWR, USA
Infrared Spectrometer	Thermo Fischer Scientific, Nicolet 380 FT-IR, USA

3.5. Sample Analysis

3.5.1. Ellipsometry

Ellipsometry is advantageous, reliable and simple technique for the measurement of thickness of the thin films on solid surfaces (Figure 3.3). The method of ellipsometry is depend on change in the state of polarization of light upon reflecting from a surface [39]. The change in the polarization state of the reflected light beam from the sample is measured, and this change in beam polarization depends on the thickness of film. Film Sense FS-1 Multi-Wavelength Ellipsometer is used in this study. Ellipsometric data is collected using 4 different wavelengths at 465 nm (blue), 525 nm (green), 590 nm (yellow) and 635 nm (red) at the same time. The wavelength and polarization state of the incident beam is set, the polarization state of the reflected beam is measured using a method called DOAP (Division-of-amplitude photopolarimeter). This method can be expressed as a matrix equation in Equation 3.2,

$$I = AS \tag{3.2}$$

where I is a 4x1 matrix showing four different intensities measured by the detector, A is a 4x4 instrument calibration matrix, and S is a 4x1 vector consisting of stoke parameters, where light polarization is expressed by four different stoke parameters S0, S1 , S2 and S4. Data on ellipsometry are quantitatively analyzed using fitting based on a model. A multilayer model is created in which the refractive index information for the substrate and polymer layers is used as inputs and the thickness of the layers is used as fit parameters. The Marquardt-Levenberg algorithm is used to detect the global minimum during the fit process. The difference between fit and measured data is defined as a fit difference and this difference is kept as small as possible.

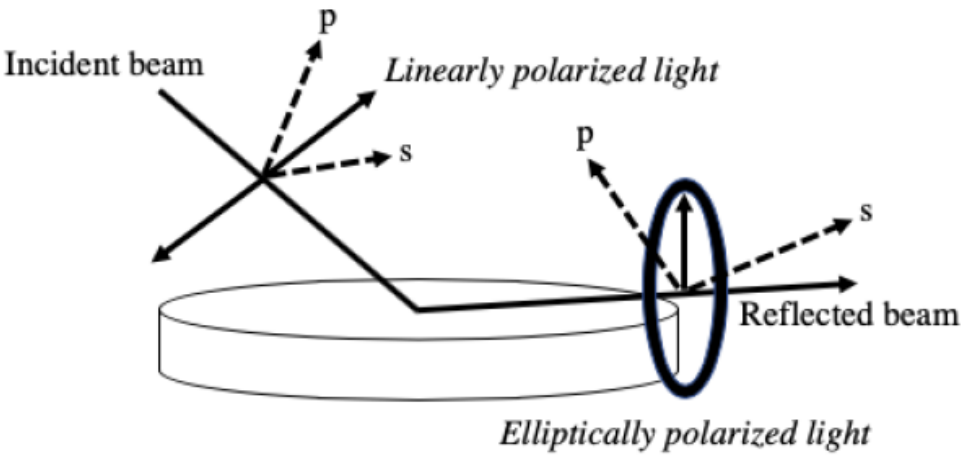

Figure 3.3. Incident light interaction with sample and polarization shifts in the ellipsometry measurement.

3.5.2. X-ray Reflectivity

Specular X-ray reflectivity (XR) measured by a tube source is a nondestructive surface characterization technique. It provides information about the structure of thin films in perpendicular direction to the film surface. It is a very reliable technique for measuring thickness of the layers as well as interfacial and surface roughnesses. Quantitative analysis of an XR curve provides electron density or scattering length density profile.

Specular X-ray reflection occurs when the incidence angle is equal to the angle of reflection (Figure3.4). In this case, there is only one component of the momentum transfer wave-vector which is in the z-direction (q_z). Therefore, gathered structural information yields the electron density variation in the perpendicular direction to the film surface, and all the structural information in x- and y-directions is averaged out during the measurement. XR is extremely sensitive to minor changes in the shape of electron density profile and hence rather small layerings or changes in the z-direction

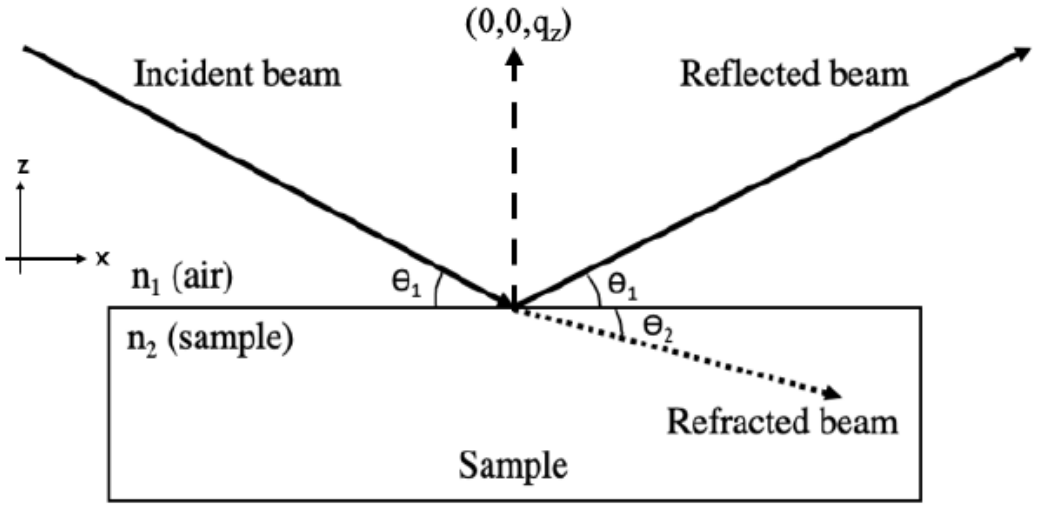

Figure 3.4. Specular X-ray reflectivity

can be resolved in great detail. q_z depends on the angle of incidence beam (θ) and the wavelength of the X-ray source (λ) as shown in the formula below;

$$q_z = \frac{4\pi Sin\theta}{\lambda} \tag{3.3}$$

Since the wavelength of the tube source is fixed, the reflectivity profile as a function of q_z is measured by simultaneously increasing the angles of incident and reflection. Reflectivity is defined as the number of reflected X-ray photons detected by a scintillation counter divided by the number of incident X-ray photons over the sample. Total external reflection for which reflectivity is equal to 1 is observed for incidence angles below the critical angle (θ_c). The X-ray beam starts penetrating into the sample at angles above θ_c, and the reflectivity decreases sharply first then following q^{-4} dependence for sharp interfaces based on Porod's law [40]. Even with a small increase in incidence angle above critical angle causes penetration depth to reach micrometers. Besides penetration depth, the probed length scale also decreases as the angle of incidence increases. As fixed beam height is used in horizontal geometry X-ray

reflectometer in this studys, the footprint of the beam on the sample decreases from centimeters to milimeters as the angle of incidence increases. Therefore, the samples have to be isotropic and uniform. Otherwise, one can observe different thicknesses or structure based on different parts of the reflectivity curve.

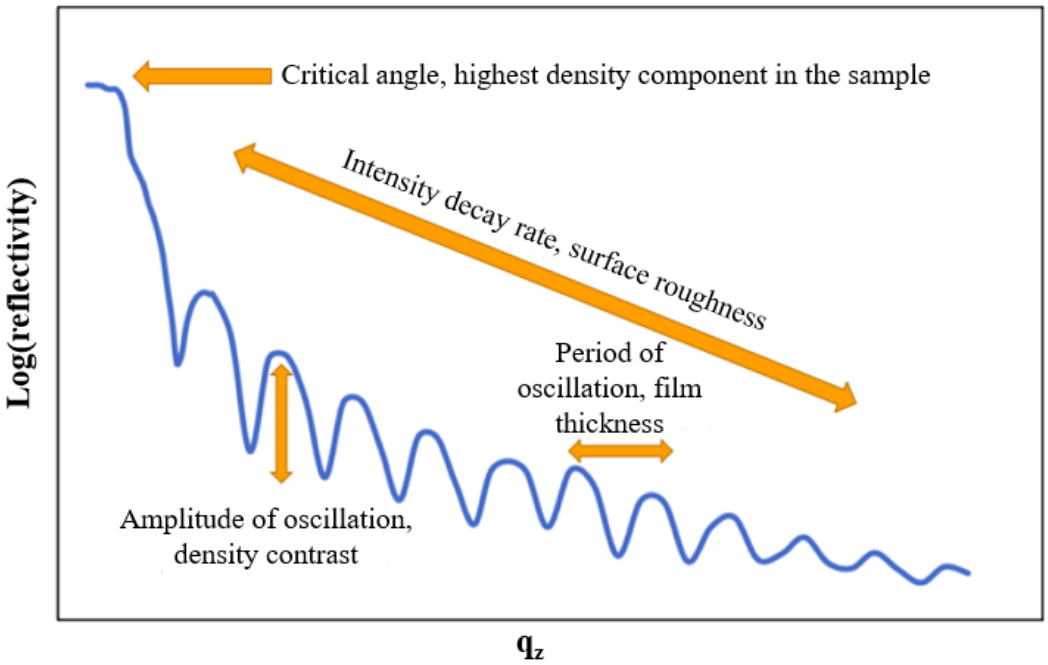

Figure 3.5. A typical profile of X-ray reflectivity that summarizes the parameters of the model and what they define in a measurement.

If a thin polymer film consists of layers with different electron densities, there is a phase difference between the reflected beams from various interfaces. Reflected waves with different phases interfere with each other constructively and destructively to form Kiessig fringes (Figure 4.2). Since the phase difference depends on the separation distance between the layers, the q_z difference between two consecutive minima or maxima can be used to estimate thickness as long as these fringes are chosen far away from critical edge to avoid dynamic effects. There is an inverse relationship between layer thickness, d_L, and fringe spacing as shown in the following equation;

$$d_L = \frac{2\pi}{\Delta q_z} \tag{3.4}$$

As the fringe spacing becomes smaller, the layer becomes thicker, or vice versa. This simple equation does not take into account the dynamic effects in the vicinity of the critical angle and it is important to use Bragg's equation [41] to obtain more precise information about the thickness without a comprehensive fit.

$$sin^2\theta_{\mathrm{i}} = \theta_c^2 + (n_i + \Delta n)^2\lambda/4d^2 \tag{3.5}$$

Where θ_{i} is the position of the maximum or minimum of the its interference fringe, θ_{c} is the critical angle, n is an integer, Δn = 1/2 and 0 for the maximum and minimum, respectively. Finally, λ is the X-ray wavelength of the copper Kα (1.54 nm) and d is the thickness.

The electron density (ED) of the adsorbed layers provide a crucial information on the density of the adsorbing chains and therefore their conformation on the surface. ED of the layers can be derived from a reflectivity measurement through fitting process. ED is directly associated with the mass density and the number of electrons in the molecule. As can be seen from eq. 3.6, the molecule's electron density also increases as the number of electrons or mass density increases. Scattering length density (SLD) is defined as the sum of scattering lengths ($\mathrm{b_i}$) for individual atoms divided by the molar volume of the molecule. In eq. 3.6, N is the number of atoms in a unit cell and Vm is the volume of the unit cell or molecule. (SLD value is proportional to electron density).

$$SLD = \frac{\Sigma_{i=1}^{N} b_i}{V_m} \tag{3.6}$$

Observing the critical angle value and the amplitude of the Kiessig fringes can give qualitative information about the SLD of the layers in the film. The layer with the largest SLD in the film determines the critical angle. Quite often thicker polymer

layers on silicon wafers have small oscillations before the critical angle for silicon and these oscillations provide details on the critical angle for the polymer layers and thus their SLDs. The relationship between the film's SLD and the critical angle is given in eq. 3.7. If the amplitude of the Kiessig fringes are large, the difference in SLD between the layers (contrast) is also large. Kiessig oscillations are dampened when the SLD contrast between the layers is weaker.

$$\theta_c = (16\pi SLD)^{1/2} \tag{3.7}$$

XR measurements are done using Bruker D8 Advance horizontal sample geometry reflectometer. Copper source has a wavelength of 0.154 nm and it is operated at a power of 1.6 kW using 40 kV bias voltage and 40 mA filament current. The beam width is 10 mm and the beam height is 0.1 mm. XR is measured up to q_z value of 0.4 $Å^{-1}$. Off-specular scattering and scattering from the substrate are measured using background scans on both sides of the specular peak and then subtracted from the raw reflectivity measurement to get true specular reflectivity. Subtracted reflectivity is normalized with the main beam intensity at the end and then this final data is fit using REFLPAK software.

Data fitting is necessary to obtain quantitative information about the thickness and SLD values of the layers, and roughnesses at each interface. Since the phase information is lost during the measurement, it is not possible to directly invert reflectivity profile to SLD profile in real space. Instead a model SLD profile built with thickness, roughness and SLD parameters that are guessed based on other preliminary characterization techniques such as ellipsometry gives approximate thickness values or AFM provides roughness at the air surface. Then a reflectivity profile is calculated from the model SLD profile and compared with the experimental reflectivity curve. Parameters in the model profile are varied till calculated and experimental reflectivity curves are in good agreement using non-linear regression. A chi-square value represents the quantitative difference between the model reflectivity and experimental reflectivity curves.

Fitting protocol in some cases cannot provide a unique model. There may be a few models that have similar chi-square values and in these cases preliminary information about the sample help to eliminate some of these models.

3.5.3. Infrared Spectroscopy

The polymer film samples were dried at vacuum oven before analysis. Background was measured with SiO_x wafer with polymer on them and polymer film samples were measured by Thermo Fisher Scientific Nicolet 380 FTIR with ATR apparatus. 64 scans were applied and resolution was 2.

4. RESULT AND DISCUSSION

Adsorption behavior of methacrylate based polymers with different side chain length and stiffness on hydrophobic passivated silicon (Si-H) and hydrophilic SiO_x surfaces studied in this thesis. All the polymers used in this work and their physical properties are given in Table 3.1. Increasing length and the stiffness of the alkyl side chains known to cause an increase in the hydrophobicity in methacrylate based polymers [31]. We have investigated the thickness and growth kinetics of adsorbed layer using ellipsometry, layer structure by X-ray reflectivity (XR), and the extent of the competing side reactions using attenuated total reflectance - infrared spectroscopy (ATR-IR).

4.1. Adsorption Kinetics on Hydrophilic and Hydrophobic Surfaces

As a reference, the growth kinetics of poly(methyl methacrylate) (PMMA) is monitored on both Si-H and SiO_x surfaces using ellipsometry and the results are shown in Figure 4.1 as a function of annealing time at T_g + 50 °C. The thickness of the adsorbed PMMA layer increases rapidly at short annealing times (< 12 h) and then continues to increase rather slowly and reach a plateau. Adsorbed PMMA layer continues to grow over Si-H surface and yield roughly 7.5 nm thickness after 120 h of annealing whereas it reached its equilibrium value of 5.5 nm on SiO_x surface in 48 h. It is quite interesting that the difference in the adsorbed layer thickness on these surfaces is not large. PMMA adsorbs on both surfaces quite well. This behavior is not consistent with the adsorption of PS on the same surfaces. In fact, polystyrene (PS) adsorbs onto Si-H surfaces with equilibrium layer thickness value almost two to three times larger than that on SiO_x surfaces [42]. This is an expected behavior since the interaction of the polymer segments and the surface plays a very important role on the adsorption.

PMMA adsorbs onto SiO_x surface with strong affinity due to hydrogen bonding between carbonyl oxygen on the side chain and hydroxyl group on the substrate surface. Rather thick adsorbed layer of PMMA on Si-H surface can be explained by two

scenarios. The first explanation is that PMMA can adsorb to Si-H surfaces with Van der Waals interactions through the backbone or side chains and the strength of these interactions are high. The other scenario implies the regrowth of native oxide layer after HF etching. If this is the case then one should not expect to see much difference on the growth kinetics and the adsorbed layer thickness. However, the differences in the growth kinetics suggest that this scenario is not likely.

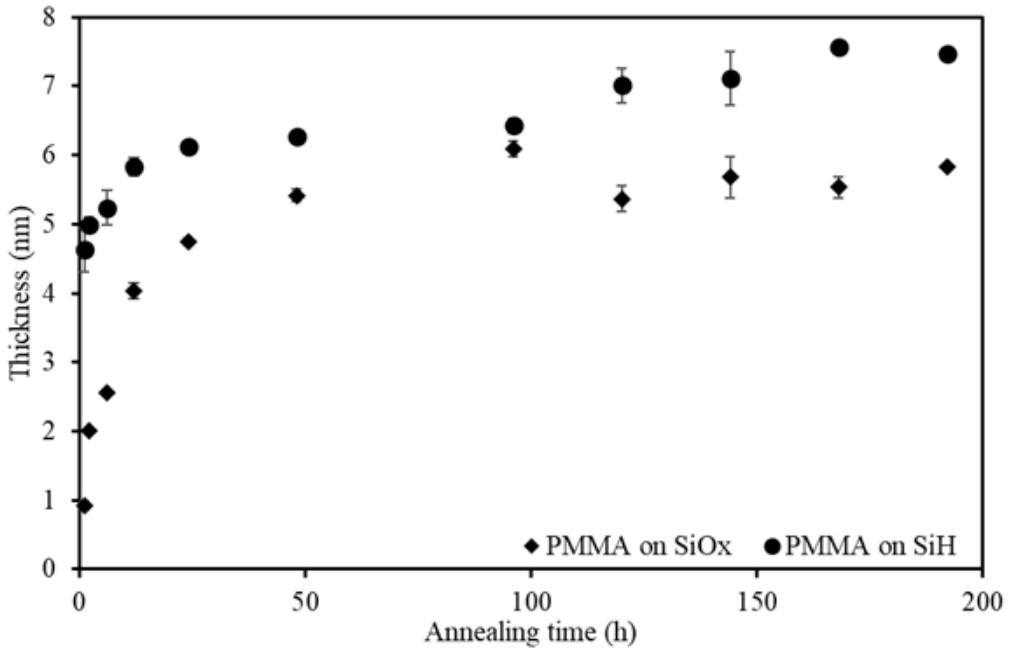

Figure 4.1. Adsorbed layer thickness as a function of annealing time at T_g + 50 °C for PMMA on SiO_x(diamonds) and on Si-H (circles).

Once the adsorption protocols are established and PMMA growth kinetics and equilibrium adsorbed layer thickness are found to be consistent with the literature [14], the adsorption process of poly(n-butyl methacrylate) (PnBMA)is is investigated. PnBMA has a 4 carbon butyl side group instead of one carbon methyl group in PMMA. Both polymers have similar molecular weight and therefore, the effect of side chain length on the adsorption can be clarified. As the number of carbons in the aliphatic side chain increases, hydrophobicity of the polymer compared to PMMA increases as well [31]. An expected consequence of increasing side chain length would be to in-

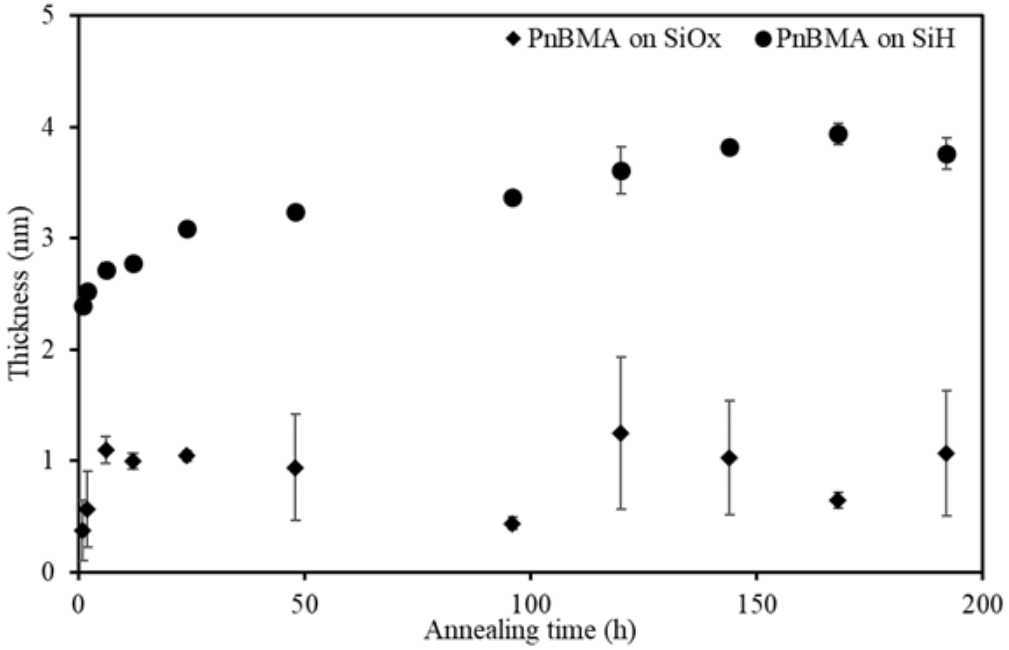

Figure 4.2. Adsorbed layer thickness as a function of annealing time at T_g + 50 °C for PnBMA on SiO_x(diamonds) and on Si-H (circles).

hibit the adsorption of PnBMA on the hydrophilic substrate due possibly to weakened ability to make hydrogen bonding interactions. PnBMA adsorbed layer thickness on SiO_x starts with 0.4 nm after 30 min annealing at T_g + 50 °C and reaches 1.09 nm after 192 h of annealing as shown in Fig. 4.2. Whereas on Si-H, it starts from 2.4 nm and reaches nearly to 4 nm thickness. The evolution of adsorbed layer thickness as a function of annealing time on Figure 4.2 demonstrated that the equilibrium adsorbed layer thickness decreases relative to PMMA on both substrates. Adsorbed PnBMA layer on Si-H is almost four times thicker than that on SiO_x at equilibrium. These results demonstrated that the interaction of PnBMA is much weaker than PMMA with both surfaces, though the hydrogen bonding ability of PnBMA is dramatically reduced. This result does not support just an increase in hydrophobicity since increasing hydrophobicity should have caused a stronger substrate-segment interaction on Si-H surface. However, this is not experimentally observed. Observed behavior raises the question about the contribution of backbone segments and side chain segments to the segment-substrate interactions. Decreased adsorbed layer thickness on both substrates may imply backbone segments are not able to interact with substrate as effectively as

in the case of PMMA due to presence of longer side chains. We will continue to test this hypothesis with other polymers which have different side chain lengths.

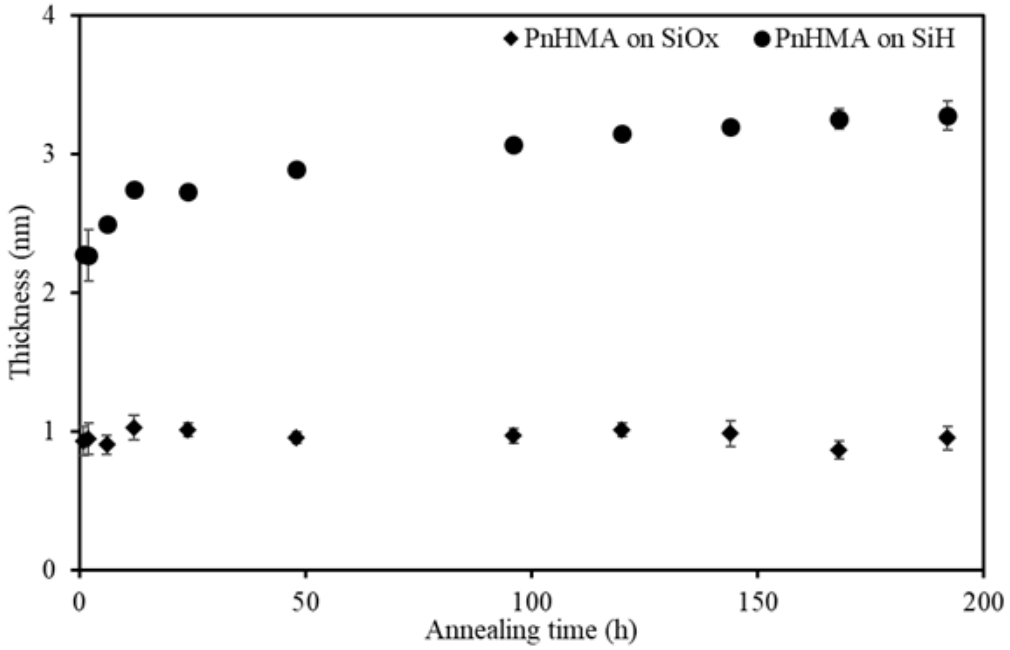

Figure 4.3. Adsorbed layer thickness as a function of annealing time at T_g + 50 °C for PnHMA on SiO_x(diamonds) and on Si-H (circles).

Further increasing side chain length to 6-carbon units using poly(n-hexyl metha crylate) (PnHMA) leads to similar adsorption behavior as PnBMA on SiO_x surface. Equilibrium adsorbed layer thickness is only 1 nm after 192 h annealing at T_g + 50 °C as shown in Figure 4.3. However, on Si-H surface the thickness of the adsorbed layer is approximately 3 nm. This is slightly lower than that of PnBMA and the thinnest between these three polymers. Clearly, as the length of the side chain increases, i.e. as the hydrophobicity of the overall chain increases, the adsorbed layer thickness decreases. This statement seems to be counterintuitive on a hydrophobic surface since one would expect to observe increased Van der Waals interactions between the PnHMA segments and Si-H substrate compared to PMMA and Si-H. However, increasing segment-substrate interaction energy can also cause more chains to adapt train conformation instead of tails and loops compared to PMMA and PnBMA. Ad-

sorbed chains can be flattened due to many contact the chain has with the underlying substrate and hence thickness of the layer will be lower. Between these two possible scenarios, so far our data supports the weakening of segment-substrate interactions due to screening between the main backbone and the substrate. Only sum frequency generation (SFG) measurements at the buried interface can reveal the distribution of chain conformations and their relative ratio right next to the substrate.

After determining increasing side chain length causes a decrease in the thickness of the adsorbed layer, we wanted to investigate the role of polymer chain tacticity on the structure and formation kinetics of the adsorbed layer. Figure 4.4 demonstrates the growth kinetics of isotactic poly(t-butyl methacrylate) (i-PtBMA) as a function of annealing time at T_g + 50 °C. The results of the same measurement is plotted in Figure 4.5 for atactic PtBMA (a-PtBMA) at 59 °C. Using PtBMA also gives us a chance to illuminate the effect of chain stiffness since the adsorption of PnBMA has been measured. Moving from 4-carbon linear side chain to bulky tertiary butyl group increases the stiffness of the chain. Comparison of Figure 4.4 and 4.5 indicates that the tacticity does not have any effect on the thickness of the adsorbed layer. The structure of the adsorbed layer and how it is affected from the tacticity will be discussed later in this section through XR meausrements. When Figure 4.2 is compared with Figure 4.5 it is obvious that the stiffness has an impact on adsorption. Increasing stiffness caused an increase on the thickness of the adsorbed layer on Si-H. However, the thickness of the adsorbed layer remains the same on SiO_x surface within the error. Thickness increase of 2 nm of a-PtBMA compared to PnBMA on Si-H layer can be explained by the bulkiness of tertiary butyl groups. These bulky side groups can prevent the formation of many segment-substrate pinning and cause more loop and tail conformations and therefore an increase in the thickness of the layer. On the SiO_x surface there is no difference between the adsorption of PnBMA, PnHMA and a-PtBMA. Independent of the bulkiness of the side chains, the ability of making hydrogen bonding with the SiO_x surface is reduced significantly.

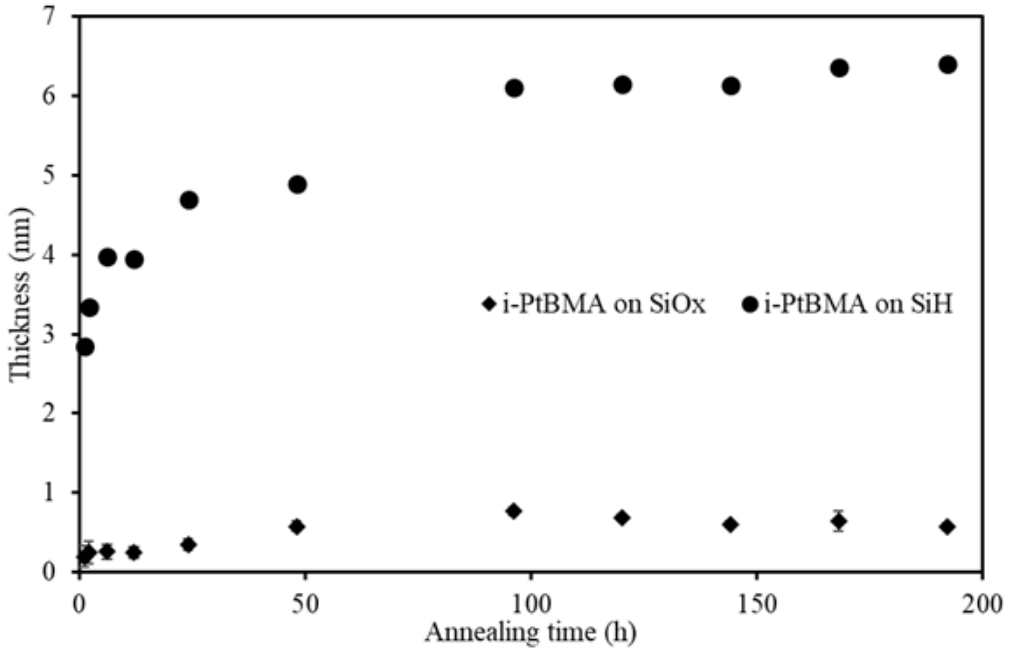

Figure 4.4. Adsorbed layer thickness as a function of annealing time at T_g + 50 °C for i-PtBMA on SiO_x(diamonds) and on Si-H (circles).

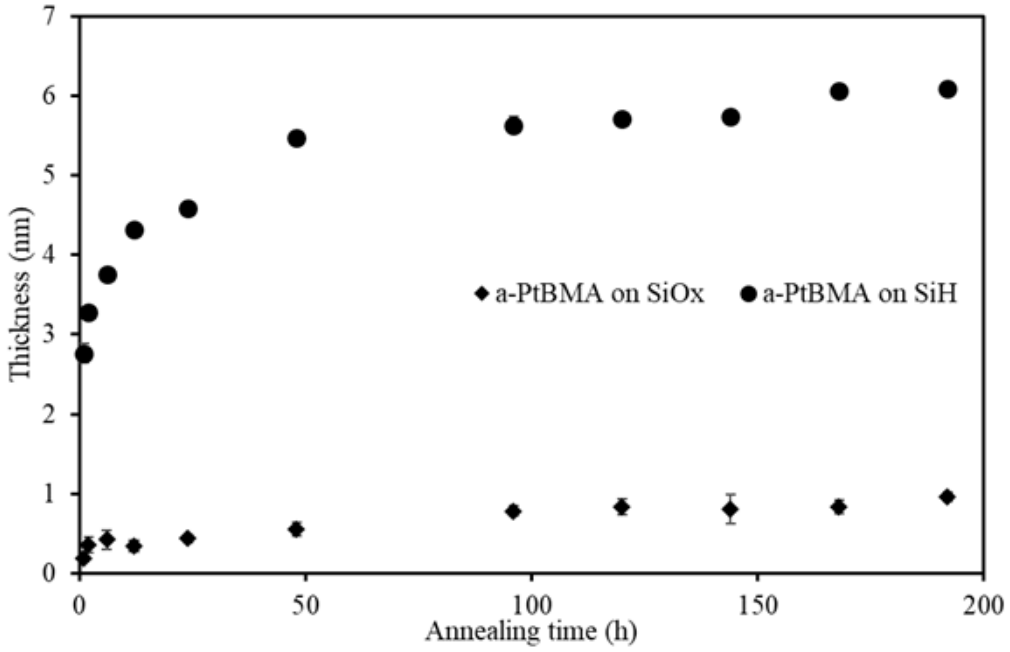

Figure 4.5. Adsorbed layer thickness as a function of annealing time at T_g - 59 °C for a-PtBMA on SiO_x(diamonds) and on Si-H (circles).

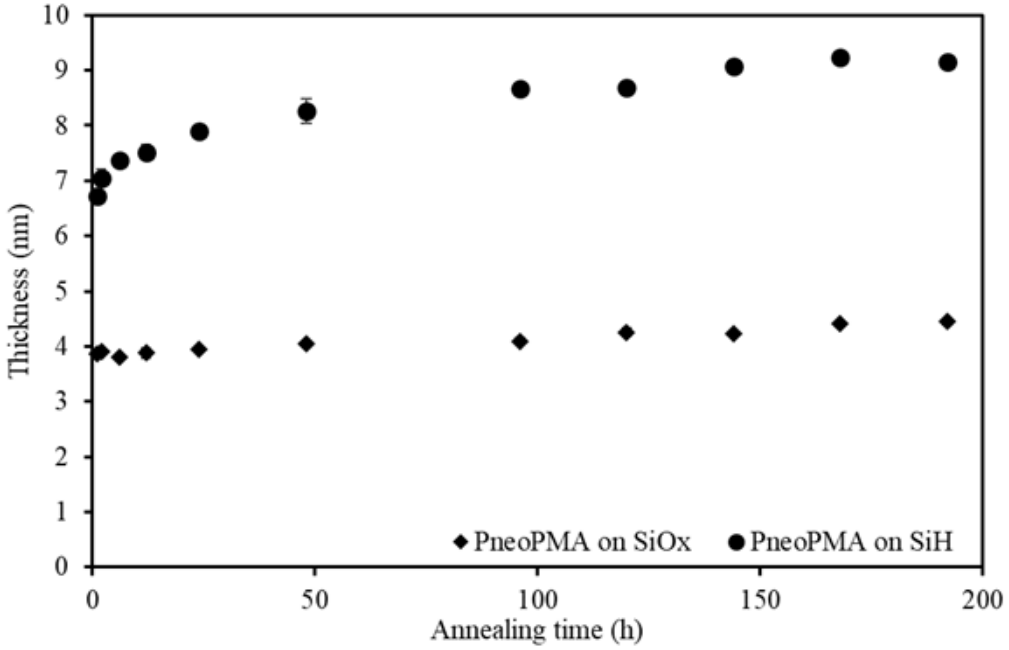

Figure 4.6. Adsorbed layer thickness as a function of annealing time at T_g + 50 °C for PneoPMA on SiO_x(diamonds) and on Si-H (circles).

Interestingly, the equilibrium adsorbed layer thickness of poly(neopenthyl metha crylate) (PneoPMA) (Fig. 4.6) is larger than the rest of the polymers on Si-H surface and only smaller than the PMMA on SiO_x surface. In fact, equilibrium thickness of PneoPMA is 4 times larger than that of a-PtBMA on SiO_x even though PneoPMA has only one more $–CH_2$ group on side chain between oxygen and bulky tertiary alkyl groups compared to a-PtBMA. At this point we are not completely sure why the thickness of the layer increases so much with the addition of a single alkyl unit, however this shows that the thickness of the adsorbed layer is influenced by small variations in the side chain. Dramatic increase in the thickness on SiO_x implies that PneoPMA is able to form hydrogen bonding with underlying substrate. This can only be possible when the carbonyl oxygen and oxygen on the side chain are able to interact with the hydroxyl groups on the substrate. It is not clear though how these oxygens are not screened by the bulky tertiary group nearby. The thickness of adsorbed PneoPMA layer is the highest on Si-H insinuated that there should be additional interactions between the side chain segments and the substrate since PMMA with mainly backbone segment-

substrate interactions only yield approximately 7 nm thick layer. We can't specify which functional groups are playing important role in these interactions yet.

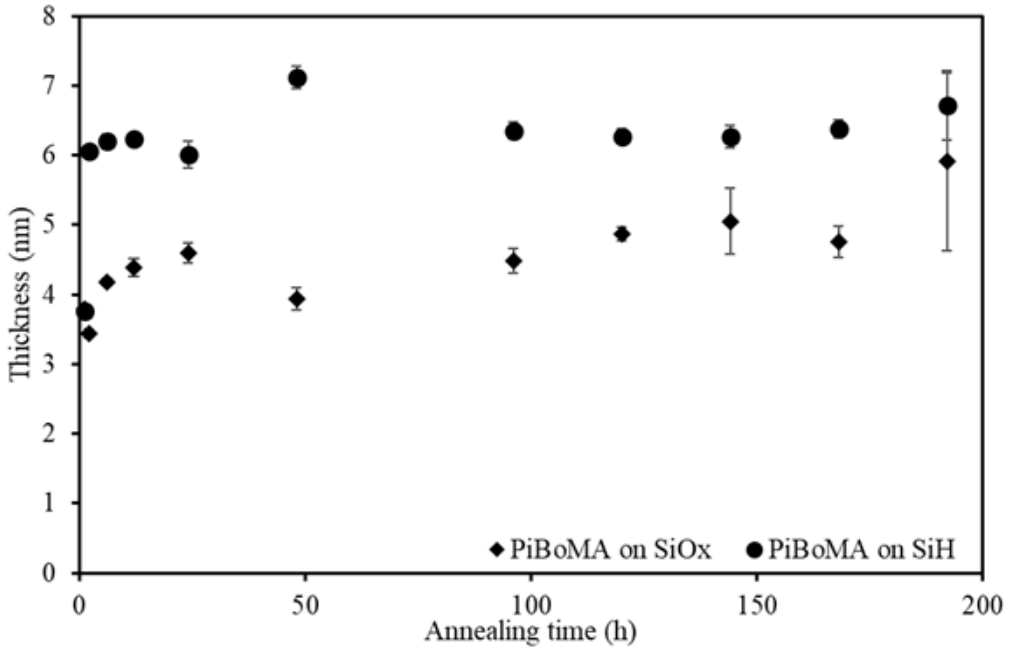

Figure 4.7. Adsorbed layer thickness as a function of annealing time at T_g - 20 °C for PiBoMA on SiO_x(diamonds) and on Si-H (circles).

The stiffest polymer in this series is poly(isobornyl methacrylate) (PiBoMA). It has a T_g value of 201 °C. Since T_g + 50 °C is higher than the high temperature limit of the vacuum oven used in this study, the adsorption measurement has been done at 180 °C which is below T_g value of PiBoMA. In this case it is expected to observe slower adsorbed layer formation and this is exactly what we can see in the adsorbed layer thickness vs annealing time plot (Figure 4.7). Adsorbed layer thickness for PiBoMA on SiO_x continued to increase up to 192 h and we could not reach the equilibirium thickness. Shape of the adsorption curves indicated that if longer annealing times are reached, the adsorbed layer thickness on SiO_x surface may exceed that on Si-H surface. Even though the adsorbed layer thickness of PiBoMA is less than that of PneoPMA on Si-H surface, this may be resulted from the lower annealing temperature. In order to compare the adsorbed layer thickness of PiBoMA with other polymers, adsorption

experiments should have been done at 250 °C . Unfortunately, our equipment cannot achieve this temperature safely. Our experiments on PS chains on similar surfaces indicated in unpublished work that the adsorbed layer thickness can be as much as two times larger when it is annealed at T_g + 50 °C compared to annealing temperatures below T_g.

4.2. X-ray Results for Adsorbed Layer

The layer structure of methacrylate based adsorbed polymer layers is investigated using X-ray reflectivity (XR) measurements. We have only measured the XR data for samples that have already reached their equilibrium thickness (192 h). Layer thickness, interface, and surface roughnesses, and the electron density profile are obtained from the fitting analysis using REFLPAK software. REFLPAK uses XR scattering length density (SLD) values instead of electron density values and the relationship between the electron density and XR SLD is given in the following equation;

$$SLD = \frac{\Sigma_{i=1}^{N} b_i}{V_m} \tag{4.1}$$

Both SLD and electron density values are related to the mass density of the polymers and number of electrons that repeating unit has, thus, mass density profile in the perpendicular direction can be derived. We have plotted logarithm of reflectivity as a function of momentum transfer wave vector in z direction, q_z, for methacrylate based polymers. In these plots experimental data points are demonstrated as blank circles and the reflectivity from best fit models are shown with solid lines. The overlap of these two represents the goodness of the fit. SLD profiles obtained from the the best fit models are plotted against depth and it shows the variation of density of the layer along the z-direction.

Table 4.1: Calculated X-ray SLD values for all polymers studied in this work and the mass densities used for calculations.

Polymer	**SLD ($Å^{-2}$)**	**Mass Density (g/cm^3)**
PMMA	1.08 x 10-5	1.16
PnBMA	9.79 x 10-6	1.05
PnHMA	9.47 x 10-6	1.01
a-PtBMA	9.51 x 10-6	1.02
i-PtBMA	9.51 x 10-6	1.02
PneoPMA	9.29 x 10-6	0.99
PiBoMA	9.88 x 10-6	1.06
PGA	1.12 x 10-5	1.24

4.2.1. XR for Adsorbed PMMA Films

The structure of adsorbed PMMA layer, as a reference, on SiH and on SiO_x surfaces has been investigated using XR. Logarithm of reflectivity as a function of momentum transfer wave-vector in z-direction, q_z, is plotted for 192 h annealed PMMA on SiO_x and SiH surfaces in Figure 4.8. Experimental data is represented with solid line and the best fits obtained from data fitting are shown as empty circles. The match between the two indicates the goodness of the fit and can be quantitatively represented by the chi-square value. The lower the chi-square value, the better the fit is. In both cases we have obtained excellent fits. The shift in Kiessig fringes to lower q_z values for adsorption on SiO_x surface demonstrates that the adsorbed layer on SiO_x surface is slightly thicker than that on SiH surface. Total adsorbed layer thickness on SiO_x is 7 nm whereas on SiH is 6.5 nm. X-ray SLD as a function of depth profiles extracted from the fitting process are illustrated in Figure 4.9.

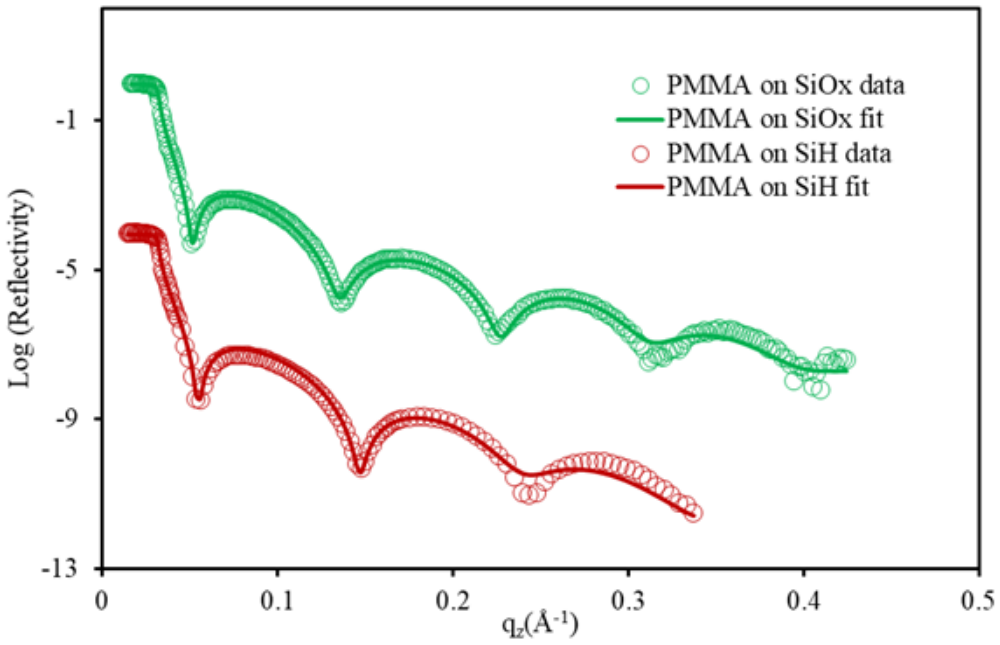

Figure 4.8. Logarithm of reflectivity as a function of q_z for 192 h annealed PMMA on SiO_x (red circles) and on Si-H (green circles). Curve for SiH surface has been shifted vertically by log $(10)^{-4}$ for clarity.

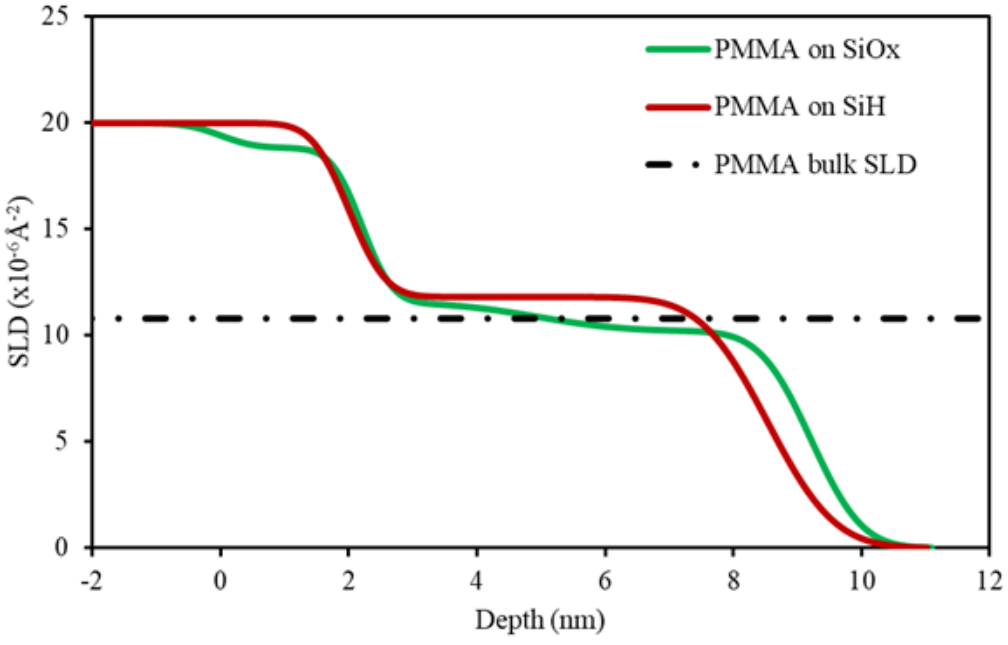

Figure 4.9. Scattering length density (SLD) as a function of depth for 192 h annealed PMMA at T_g + 50 °C on SiO_x (green) and on SiH (red).

SLD profile for adsorbed PMMA film on SiO_x surface contains four layers. At the bottom there is semi-infinite Silicon (Si) layer and its SLD value is kept constant at 2 x 10^{-5} Å^{-2} throughout the fitting. There is a SiO_x layer above the Si substrate which has a thickness of 2 ± 0.2 nm and its SLD kept constant as 1.88 x 10^{-5} Å^{-2}. First adsorbed PMMA layer is 2.7 nm thick and next to SiO_x layer. The SLD value of this layer is 1.16 x 10^{-5} Å^{-2}. The horizontal dash line in Figure 4.9 indicates the SLD value for PMMA chains in bulk. The SLD value of the first adsorbed layer is only slightly larger than the bulk value for PMMA. In the literature, it has been found that the linear polymers adsorbed to form two layers. The layer next to the substrate is composed of flattened chains which form to have a higher density layer than the bulk. Chains in this layer are the first arriving chains and they make lot of contacts with the substrate and they adapt train conformation. The second adsorbed layer contains loosely adsorbed chains since these chains arrive to the substrate later and they cannot make many segment-substrate interactions. They have a SLD value similar to the bulk value. Similar to the literature, we also observe a second adsorbed layer next to air surface with SLD value of 1.02 x 10^{-5} Å^{-2} which is less than the SLD value for the bulk PMMA. However, the SLD difference between the two layers is not large. The thickness of the adsorbed layer with higher SLD value is 2.7 nm and the thickness of the loosely adsorbed layer is 4.3 nm. SLD profile for PMMA on SiH surface has 2 layers. On top of Si substrate there is a single adsorbed PMMA layer. Adsorbed PMMA layer on top of Si is 6.5 nm thick and SLD value of this layer is 1.18 x10^{-5} Å^{-2}.

4.2.2. XR for Adsorbed PnBMA Films

Ellipsometry measurements shown in Figure 4.2 indicated that the thickness of the adsorbed PnBMA layer is higher on SiH surface. Adsorbed layer thickness of PnBMA layers on both surfaces were less than that of adsorbed PMMA layers. XR curves shown in Figure 4.10 also verifies the same fact that the adsorbed PnBMA layers are thinner. Both reflectivity curves have been fitted using single adsorbed polymer layer. XR SLD profiles obtained from the best fits are plotted as a function of depth in Figure 4.11. On SiO_x surface, adsorbed PnBMA layer is 2.65 nm thick and the SLD

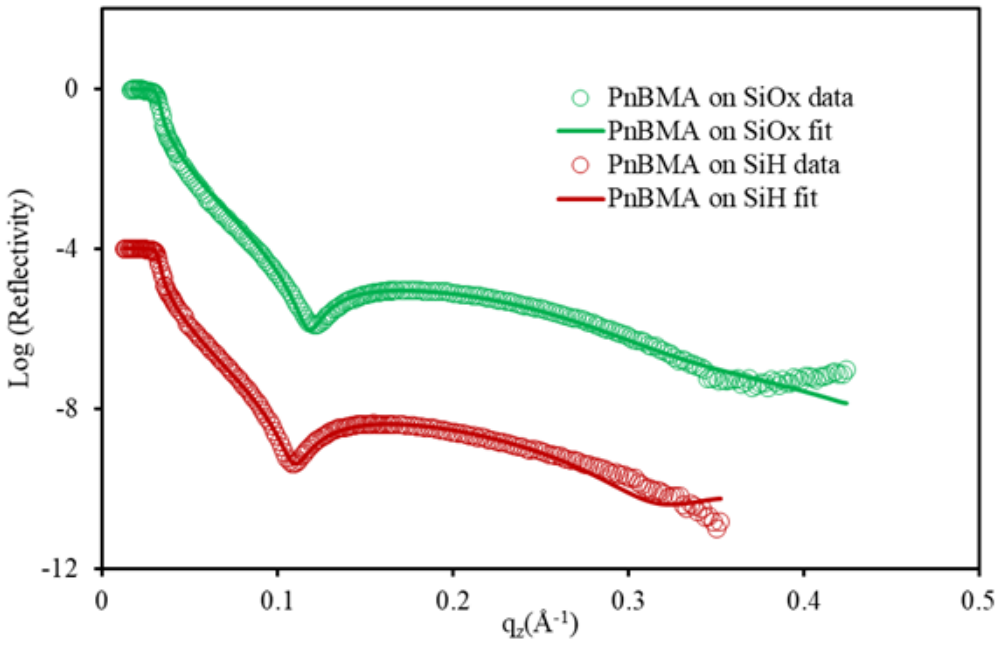

Figure 4.10. Logarithm of reflectivity as a function of q_z for 192 h annealed PnBMA on SiO_x (red circles) and on Si-H (green circles). Curve for SiH surface has been shifted vertically by log $(10)^{-4}$ for clarity.

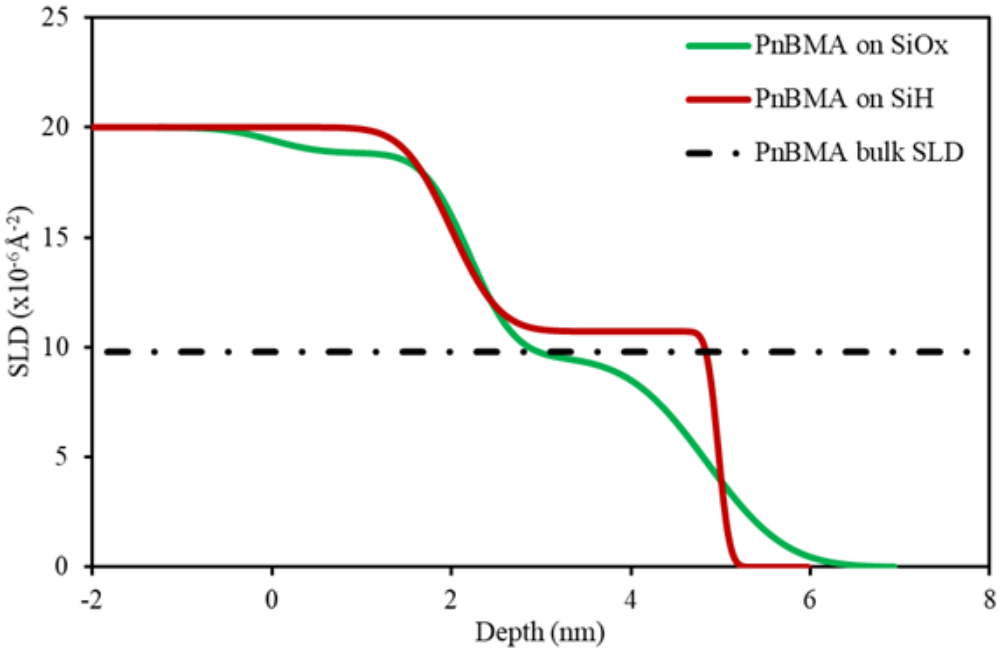

Figure 4.11. Scattering length density (SLD) as a function of depth for 192 h annealed PnBMA at T_g + 50 °C on SiO_x (green) and on SiH (red).

value is 9.56 x 10^{-6} $Å^{-2}$ which is slightly lower than the bulk SLD value for PnBMA. On SiH surface, adsorbed PnBMA layer has 2.97 nm thickness and SLD value of 1.07 x 10^{-5} $Å^{-2}$ which is above bulk SLD value. Adsorbed layer formed on SiH surface is thicker, denser and smoother than that formed on SiO_x surface. The fact that the layers are thinner than 3 nm implies the chains are most likely flattened due to many segment-substrate contact [12]. If most of the free surface sites are filled by the chains which are flattened then it may not be possible to observe loosely adsorbed chains. In this case, lack of loosely adsorbed chains cannot be due to insufficient annealing time since the thickness of the layers reached an equilibrium value much earlier than 192 h of annealing based on the ellipsometry measurements shown in Figure 4.2. The most important conclusion can be drawn from Figure 4.11 is that the thickness of the adsorbed layer decreases when the side chain length increases from 1 alkyl group to 4 alkyl groups on both surfaces.

4.2.3. XR for Adsorbed PnHMA Films

Further increasing side chain from n-butyl to n-hexyl using PnHMA leads to increase in the hydrophobicity of the polymer chain. The lack of multiple Kiessig fringes in the reflectivity data suggests that the layers are very thin. Both data sets have been fit using a single adsorbed layer model and this model yield theoretical XR curves overlapping very well with the experimental data (Figure 4.12). The XR SLD profiles obtained from the best fit models are shown in Figure 4.13. Adsorbed PnHMA layers on both surfaces are rough. Their SLD values are slightly above the bulk SLD value for PnHMA but this SLD value drops very rapidly below bulk SLD. The layers are thinner than the adsorbed PnBMA layers on both surfaces. On SiO_x surface, the adsorbed PnHMA layer has 1.6 nm thickness with SLD value of 9.53 x 10^{-6} $Å^{-2}$, on contrary, the polymer has 2.5 nm thickness on SiH surface with SLD value of 1.22 x 10^{-5} $Å^{-2}$ which is way above its bulk SLD value. As in the case of PnBMA, PnHMA also forms mostly flattened layer with a thickness value less than 3 nm. Formation of very thin and rough layer on SiO_x insinuated that the hydrogen bonding ability of PnHMA with –OH groups on the substrate is dramatically hindered.

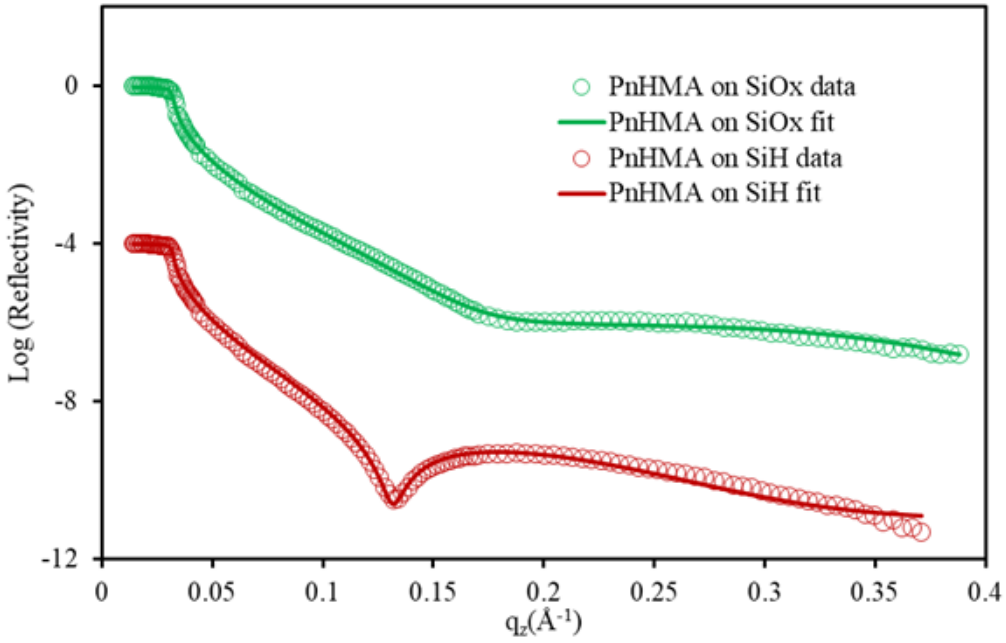

Figure 4.12. Logarithm of reflectivity as a function of q_z for 192 h annealed PnHMA on SiO_x (red circles) and on Si-H (green circles). Curve for SiH surface has been shifted vertically by log $(10)^{-4}$ for clarity.

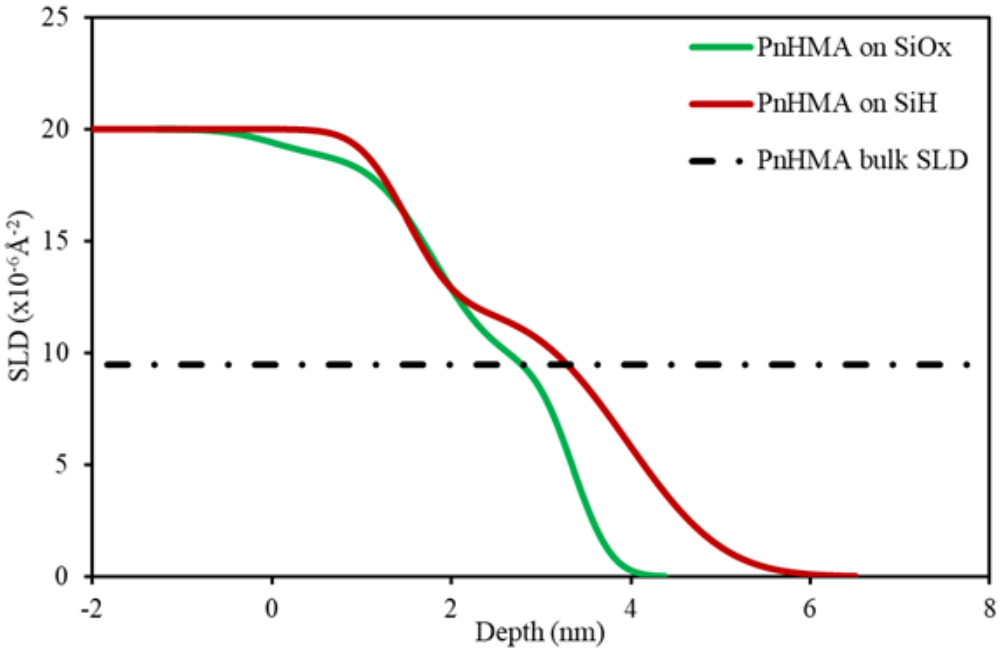

Figure 4.13. Scattering length density (SLD) as a function of depth for 192 h annealed PnHMA at T_g + 50 °C on SiO_x (green) and on SiH (red).

4.2.4. XR for Adsorbed PtBMA Films

So far, the increase in the side chain length from one methyl group to n-hexyl group resulted in thinner adsorbed layers on hydrophilic and hydrophobic surfaces. At this point, we wanted to determine the role of bulkiness on the structure of the adsorbed layer using a tertiary butyl side chain (PtBMA). At the same time, using both isotactic and atactic PtBMA in our experiments served us to elucidate the role of tacticity on the structure of adsorbed layer. Isotactic PtBMA (i-PtBMA) and atactic PtBMA (a-PtBMA) have very distinct T_g values of 9 °C and 118 °C, consecutively.

Based on the experimental protocol used for earlier measurements, adsorption experiments should be done at 60 °C for i-PtBMA and 168 °C for a-PtBMA. However, tertiary butyl groups in PtBMA and poly(tert-butyl acrylate) (PtBA) are well known to drop at high temperatures [43] [44]. For this reason, we have followed the adsorption for both polymers at 60 °C to avoid the competing side reactions. XR curves and the best fits for the 192 h annealed i-PtBMA and a-PtBMA on SiO_x and SiH surfaces are shown in Figures 4.14 and 4.15, successively. Thickness values obtained from XR data agree with ellipsometry measurements within 10%. It is obvious even from the number of fringes in the raw data that the adsorbed PtBMA layers on SiO_x are much thinner than the same layers formed on SiH surface. As in the case of n-butyl and n-hexyl, t-butyl side group inhibit the formation of thicker adsorbed PtBMA layer on SiO_x surface most likely due to reduction in the hydrogen bonding between the segment of PtBMA and –OH groups on the substrate surface. However, the thickness of the adsorbed i-PtBMA and a-PtBMA layers on SiH surface is quite close to the thickness of the adsorbed PMMA layer on the same surface. This increase in hydrophobic surface is especially interesting when it is compared with the adsorbed layer thickness of PnBMA. The number of alkyl chains on the side chain are identical and the only difference is the way these alkyl units are connected to each other. Bulkier tertiary butyl group has caused an increase in the hydrophobic interactions between the polymer chain and the substrate surface which resulted in thicker adsorbed layer.

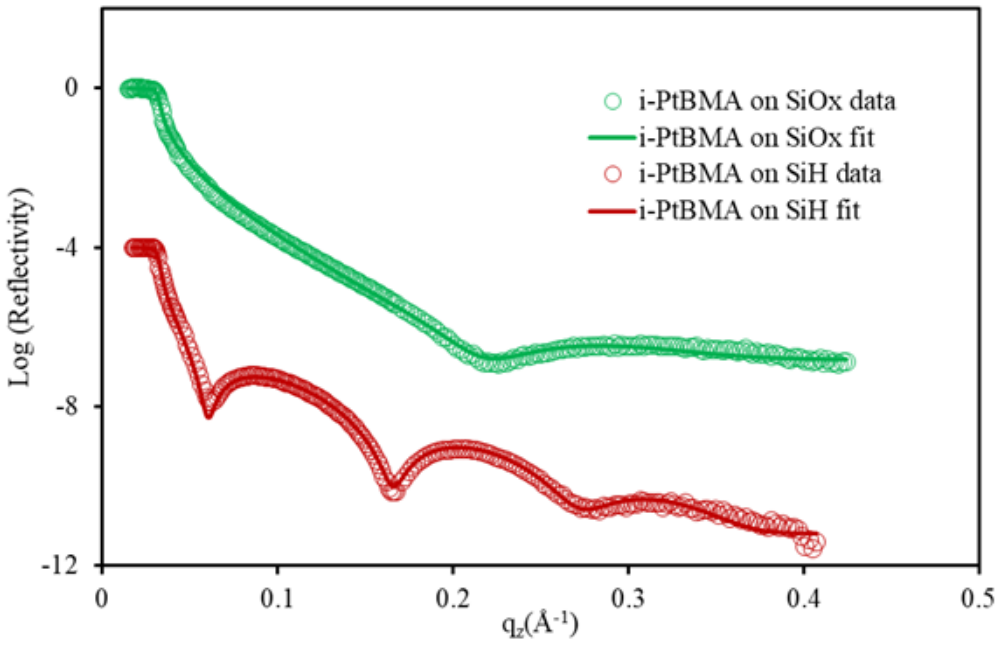

Figure 4.14. Logarithm of reflectivity as a function of q_z for 192 h annealed i-PtBMA on SiO_x (red circles) and on Si-H (green circles). Curve for SiH surface has been shifted vertically by log $(10)^{-4}$ for clarity.

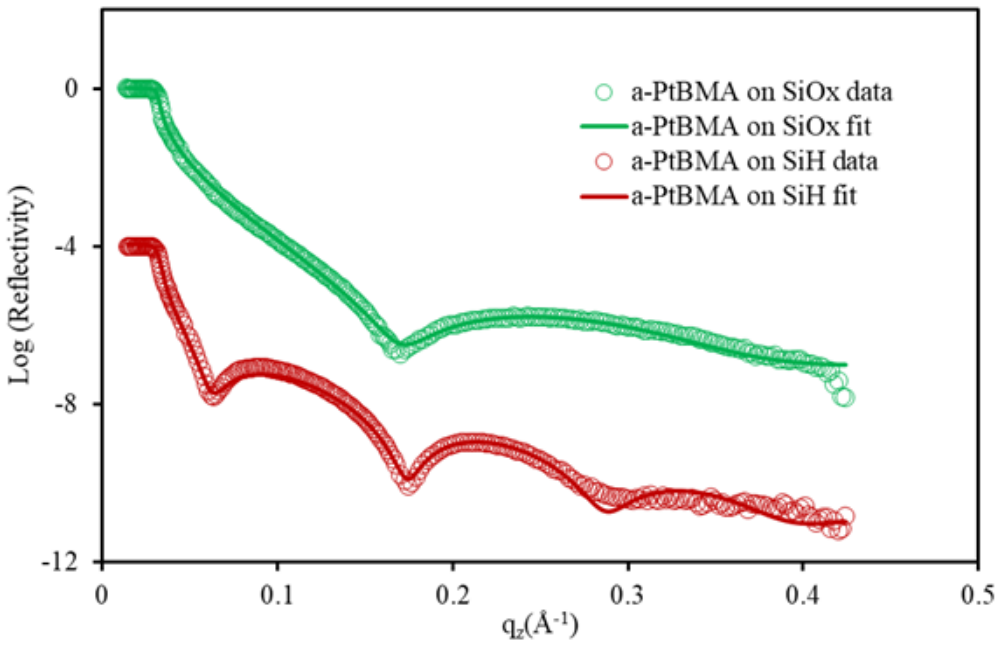

Figure 4.15. Logarithm of reflectivity as a function of q_z for 192 h annealed a-PtBMA on SiO_x (red circles) and on Si-H (green circles). Curve for SiH surface has been shifted vertically by log $(10)^{-4}$ for clarity.

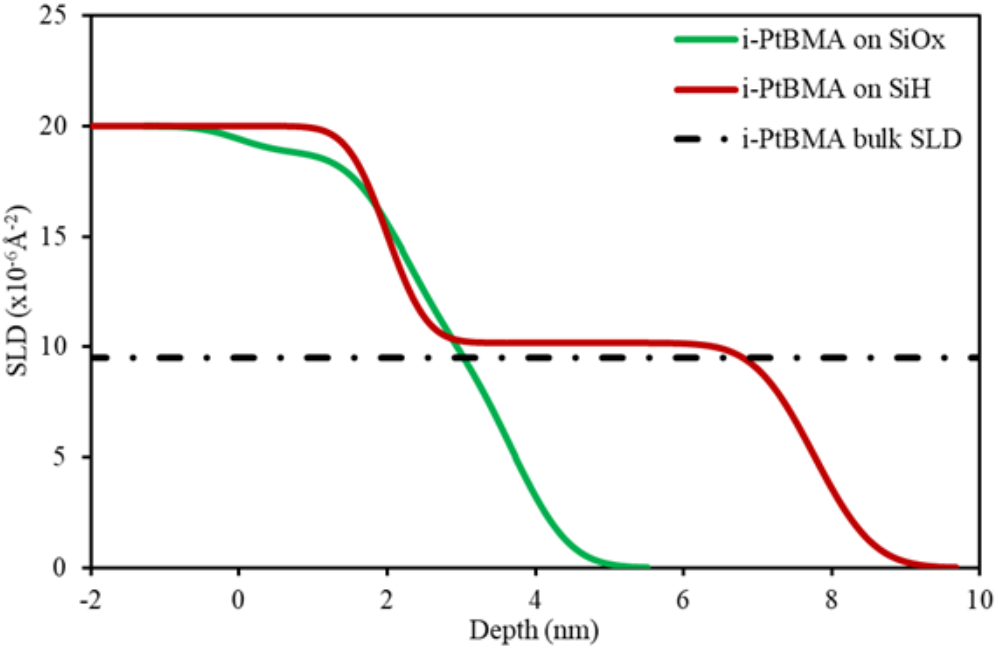

Figure 4.16. Scattering length density (SLD) as a function of depth for 192 h annealed i-PtBMA at T_g + 50 °C on SiO_x (green) and on SiH (red).

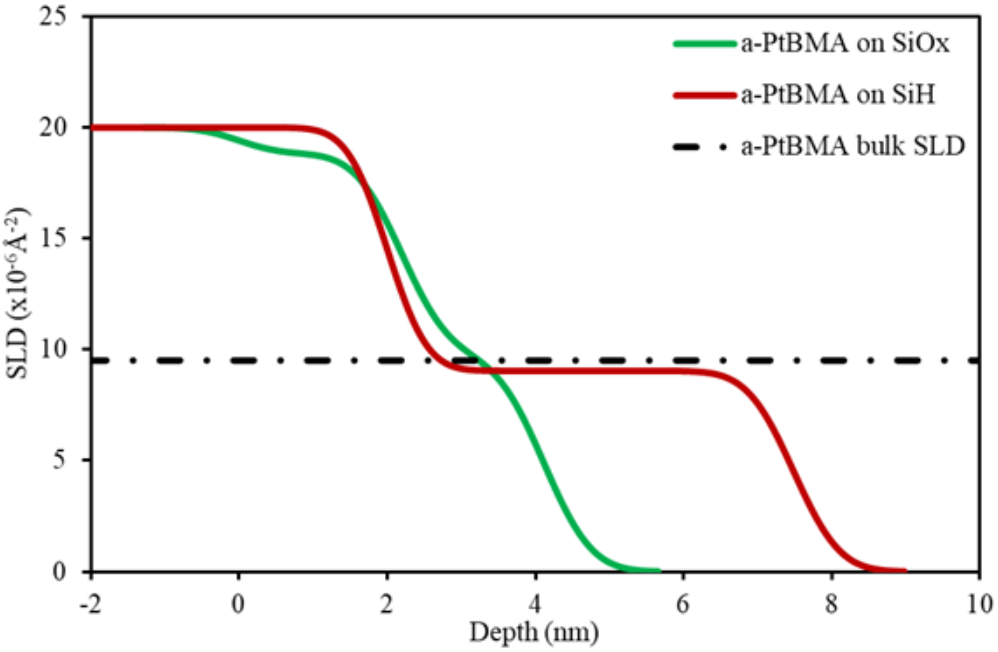

Figure 4.17. Scattering length density (SLD) as a function of depth for 192 h annealed a-PtBMA at T_g - 59 °C on SiO_x (green) and on SiH (red).

SLD profiles obtained from the best fits using single layer model shown in Figure 4.14 and 4.15 are plotted as a function of depth in Figure 4.16 for i-PtBMA and in Figure 4.17 for a-PtBMA. Adsorbed i-PtBMA layer on SiO_x surface has 1.53 nm thickness with SLD value of 1.00 x 10^{-5} $Å^{-2}$. However, the rms roughness of 1.38 nm at the air surface is relatively high for such a thin layer. The way the SLD decays from SiO_x to air surface suggests that this is not a discrete layer. Thickness of the adsorbed i-PtBMA layer on SiH surface is 5.76 nm and its SLD value is 1.02 x 10^{-5} $Å^{-2}$ which is slightly above the bulk SLD value of PtBMA. The results presented for a-PtBMA in Figures 4.15 and 4.17 are very similar to those for i-PtBMA. XR data for adsorbed layers of a-PtBMA are fit using a single layer model. This model yields 1.92 nm thickness and SLD value of 9.76 x 10^{-6} $Å^{-2}$ on SiO_x surface. On SiH, the thickness of the adsorbed a-PtBMA is 5.48 nm and the SLD of the layer is 9.04 x 10^{-6} $Å^{-2}$. This is lower than the bulk SLD value of PtBMA. We can conclude that the tacticity of the polymer does not play a significant role on the structure and formation of the adsorbed layer.

4.2.5. XR for Adsorbed PneoPMA Films

Introducing a bulky tert-butyl group next to oxygen atom in the side group significantly hindered the ability to form hydrogen bonds with –OH functional groups on SiO_x surface as explained above. At the same time, it caused a huge increase in the thickness of the adsorbed layer on a hydrophobic surface compared to its linear version PnBMA. Witnessing these dramatic changes upon introduction of tert-butyl group suggested us moving the bulky group slightly away from the oxygen and carbonyl groups to observe if the hydrogen bonding ability can be recovered. For this reason we have obtained poly(neo-pentyl methacrylate) (PneoPMA) in which there is a -CH_2 group between the oxygen and the tert-butyl group. Experimental XR curves and the best fits are plotted for 192 h annealed PneoPMA at 80 °C in Figure 4.18. There are three visible Kiessig fringes in XR data for adsorbed PneoPMA on SiO_x surface. This is a clear indication for a thicker layer compared to earlier adsorbed layers on SiO_x surface.

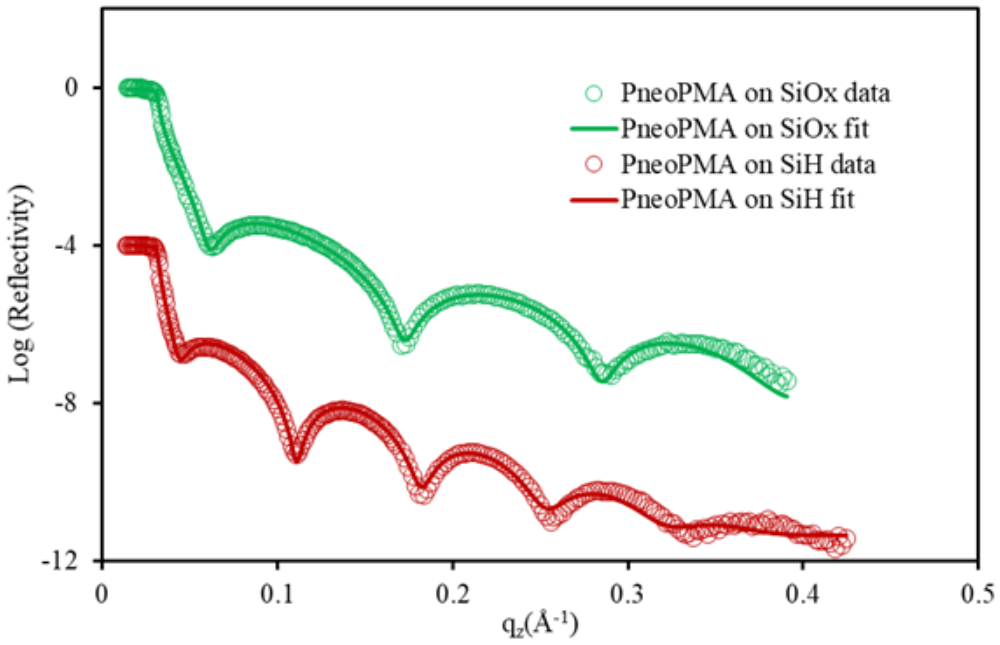

Figure 4.18. Logarithm of reflectivity as a function of q_z for 192 h annealed PneoPMA on SiO_x (red circles) and on Si-H (green circles). Curve for SiH surface has been shifted vertically by log $(10)^{-4}$ for clarity.

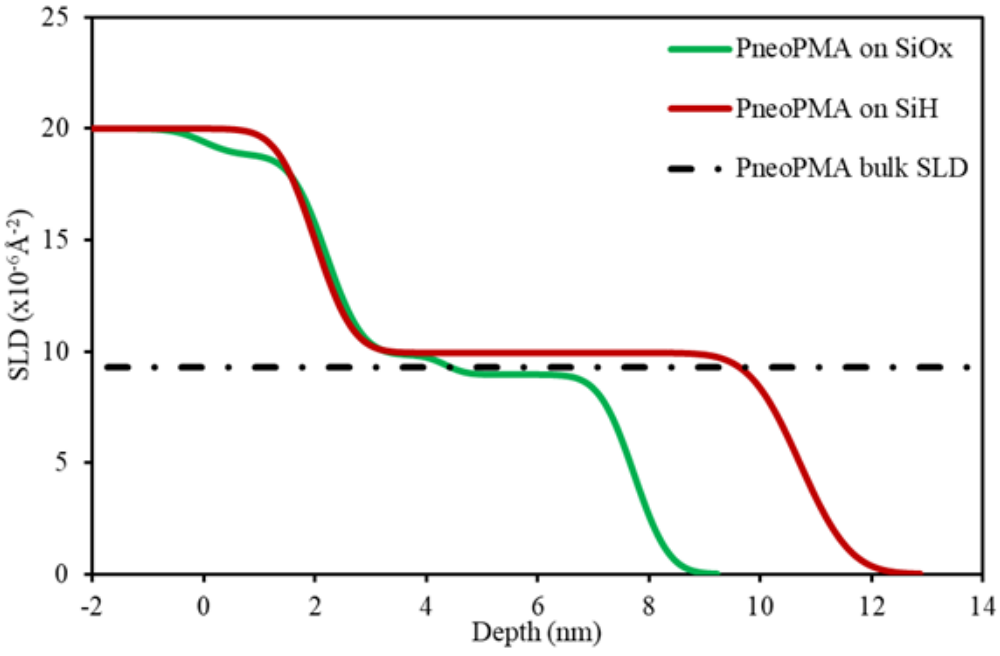

Figure 4.19. Scattering length density (SLD) as a function of depth for 192 h annealed PneoPMA at T_g + 50 °C on SiO_x (green) and on SiH (red).

The data was fit using a two-layer model and the SLD profile obtained from the model fitting is shown in Figure 4.19. Adsorbed PneoPMA layer on SiO_x surface is 5.5 nm thick in total. SLD value of the layer next to the substrate is 9.84 x 10^{-6} $Å^{-2}$ which is slightly above bulk SLD value of PneoPMA and its thickness is 2.14 nm. Second layer is atop the first layer with SLD value of 8.96 x 10^{-6} $Å^{-2}$ and thickness of 3.39 nm. The SLD of this layer is almost same as the bulk SLD value of PneoPMA. On the other hand, on SiH surface, adsorbed PneoPMA layer has 8.71 nm thickness with SLD value of 9.93 x 10^{-6} $Å^{-2}$ which is way slightly above its bulk value. This layer is well-described using a single layer model.

The thickness of adsorbed PneoPMA on SiH surface is the highest between all the polymers. Addition of a single $–CH_2$ group between the bulky tert-butyl group and hydrogen bonding functional groups reduced the steric hindrance and facilitated the hydrogen bonding between the substrate and polymer segments. It is not clear how does the addition of this group resulted in 50% increase in the layer thickness on SiH surface. However, it demonstrates that the structure of the adsorbed layer depends strongly on the chemical structure of the repeating unit.

4.2.6. XR for Adsorbed PiBoMA Films

Poly(isobornyl methacrylate) (PiBoMA)is the stiffest polymer that we have used in this study. It has a T_g value of 200 °C. Since the vacuum oven cannot reach temperatures higher than 200 °C safely, the adsorption experiments were performed at T_g - 20 °C. XR measurements and the best fits from the modelling were plotted in Figure 4.20 for 192 h annealed PiBoMA at 180 °C. It is obvious from the raw data that the XR curve for the adsorbed PiBoMa layer on SiO_x surface have more Kiessig fringes than that on SiH surface in the same q_z-range. Hence, the adsorbed PiBoMA layer is thicker on SiO_x surface. In fact, this is the only polymer that formed a thicker adsorbed layer on SiO_x surface. XR curve for the adsorbed layer on SiO_x surface was fit using a bilayer model and the SLD profile obtained from this model is plotted in Figure 4.21. The layer next to the substrate is 5.2 nm thick and it has the bulk SLD value. The layer above that has an SLD value slightly lower than bulk value and it is

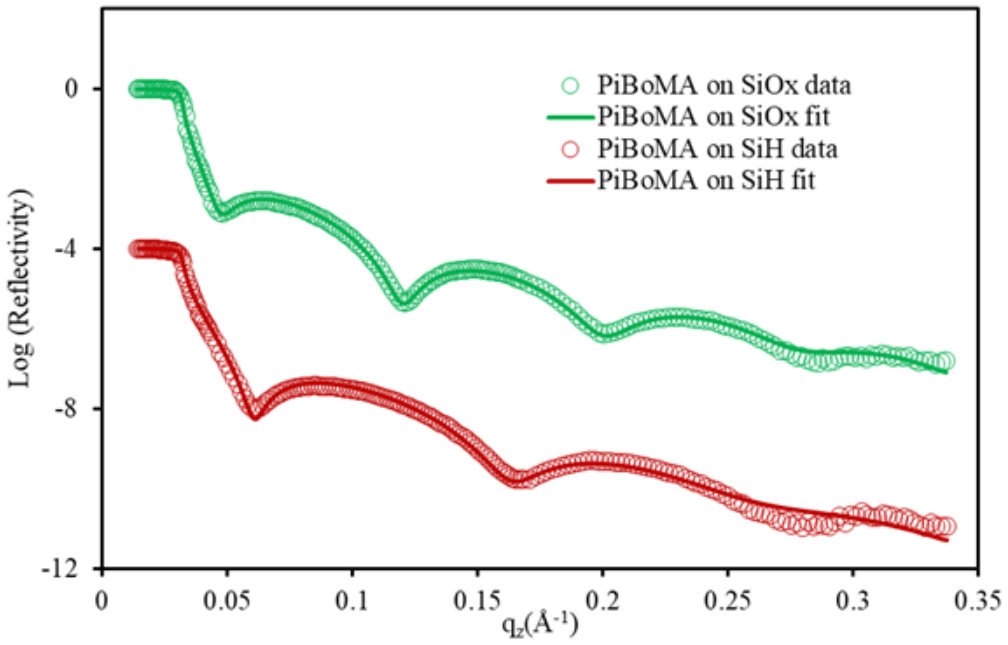

Figure 4.20. Logarithm of reflectivity as a function of q_z for 192 h annealed PiBoMA on SiO_x (red circles) and on Si-H (green circles). Curve for SiH surface has been shifted vertically by log $(10)^{-4}$ for clarity.

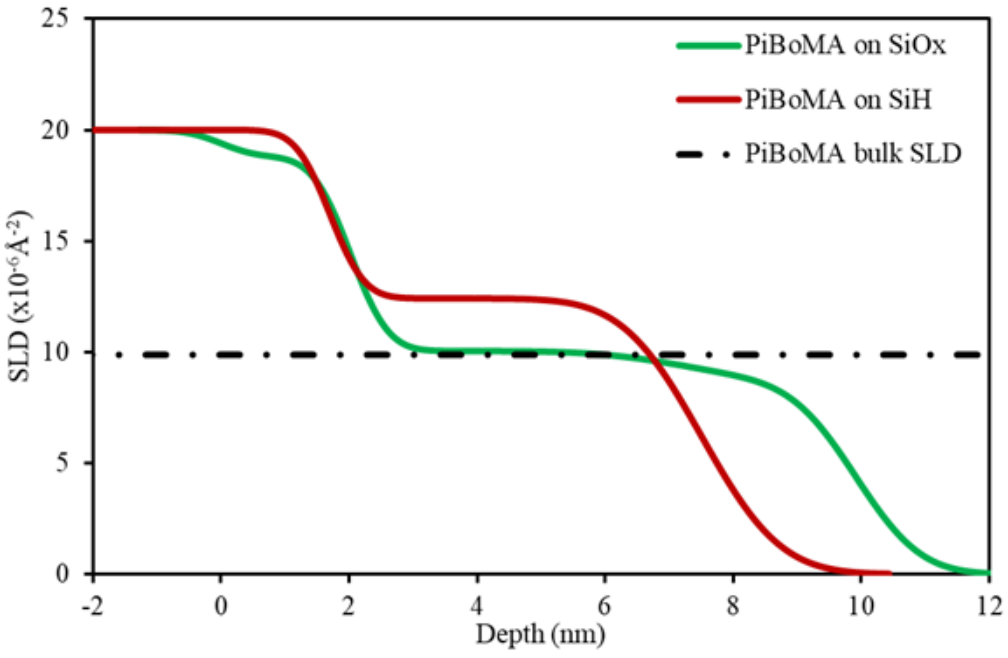

Figure 4.21. Scattering length density (SLD) as a function of depth for 192 h annealed PiBoMA at T_g - 20 °C on SiO_x (green) and on SiH (red).

2.7 nm thick. Interface roughness between these two layers is high so that the transition is smooth and gradual. The XR data for the adsorbed PiBOMA on SiH was fit by a single layer model for which the thickness is 5.8 nm and the SLD value is 1.24 x 10^{-5} $Å^{-2}$. This SLD value is roughly 25% higher than bulk SLD value of PiBoMA. Even though the adsorbed layer is thicker on SiO_x surface, it forms a denser layer on SiH surface most likely due to increase in the fraction of flattened chains. We also have to note that adsorbed PiBoMA layer on SiO_x surface did not reach its equilibrium thickness based on ellipsometry results presented in Figure 4.7. We can safely assume measured 7.9 nm thickness is a lower bound value on SiO_x surface at equilibrium. This polymer similar to PMMA yields thick adsorbed layers on both surfaces which is surprising since isobornyl group is a very bulky group attached directly to the oxygen on the side chain. Our expectation was to observe almost no layer on SiO_x surface due to steric hindrance caused by the bulky group. However, at the substrate interface a rearrangement seems to happen in such a way that the isobornyl group has almost no impact on the hydrogen bonding ability of oxygen and carbonyl groups with the substrate.

4.3. Effect of Competing Side Reactions

Earlier in section 4.2.4, we have drawn attention to the annealing temperature for i-PtBMA and a-PtBMA adsorption experiments and emphasized that same measurements should be done at temperatures higher than 120 °C to determine the equilibrium adsorbed layer thickness for a-PtBMA. However, it is a well-known fact that the tertiary butyl groups fall at this temperature and this may present a rather complicated situation in which the effect of adsorption cannot be simply retrieved. In order to understand the extent of adsorption and side reactions, we have performed ellipsometry measurements before and after toluene leaching, ATR-IR measurements and XR measurements for equilibriated samples of i-PtBMA and a-PtBMA. Thicknesses of the a-PtBMA layers annealed at 168 °C before and after toluene leaching are shown in Figure 4.22. The initial spun-cast a-PtBMA films are 46 nm on SiO_x surface and 51 nm on SiH surface. When a spun-cast polymer film is annealed above its T_g, in general there

is only 1-2% of thickness reduction due to removal of residual solvent [13]. However, in this case we observe almost 20% decrease in film thickness within the first 12 hours of annealing. This is a substantial change and it is very hard to explain with the presence of residual solvent. In fact, after 24 h of annealing film thickness drops to half of its initial value and remained same up to 120 h of annealing at 168 °C. A similar thickness decrease was observed by Treat et al. for poly(t-butyl acrylate) (PtBA) brush after 30 min heating at 190 to 200 °C [43]. Originally 36 nm thick PtBA brush is converted to 16 nm thick poly (acrylic acid) brush after the heat treatment. Our observation for the thikness reduction is in good agreement with Treat et al. and indicates that the tertiary butyl groups are removed from the film. The difference between the time scales to see the same kind of thickness reduction is due to the treatment temperature.

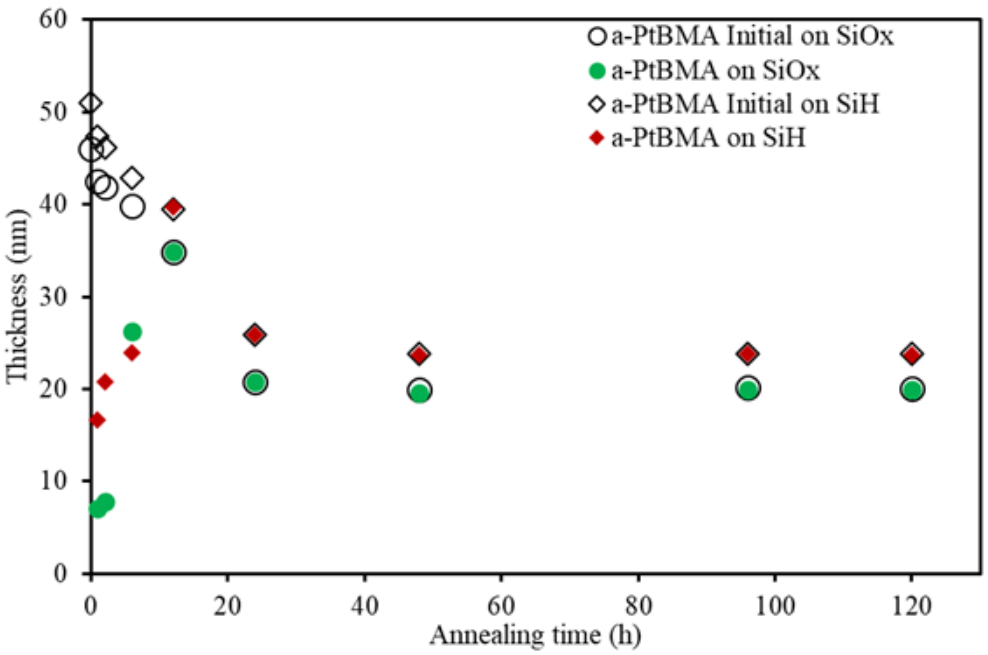

Figure 4.22. Thickness of a-PtBMA layers on SiO_x (circles) and on SiH (diamonds) surfaces before (empty symbols) and after (filled symbols) toluene leaching as a function of annealing time.

On the other hand, the thickness of a-PtBMA layers after toluene leaching increases rapidly up to 12 h of annealing then decreases and stays constant after 24 h.

These presumably adsorbed layers have initial thicknesses much higher than the adsorbed layers obtained at 60 °C. Even after 1h of annealing at 168 °C and consequent washing, a-PtBMA layers are 7 nm thick on SiO_x surface and 16.6 nm thick on SiH surface, successively. Considering the fact that the thickness of adsorbed a-PtBMA layer obtained at 60 °C on SiO_x was less than 2 nm and on SiH it was around 6 nm, very thick a-PtBMA layers raised questions about how much of the layer is composed of adsorbed chains. After 12 h of annealing, the thickness of the a-PtBMA layers before and after toluene leaching becomes identical. This insinuates that the layers do not contain any non-adsorbed chains and most-likely there is some kind of cross-linked structure. Thickness of the layers stays constant after 24 h of annealing around 24 nm on SiH surface and 20 nm on SiO_x surface. Since the ellipsometry measurements do not reveal any information about the composition or structure of the layer we have performed ATR-IR and XR measurements to determine the extent of adsorption and side reactions triggered by the fall of tert-butyl groups.

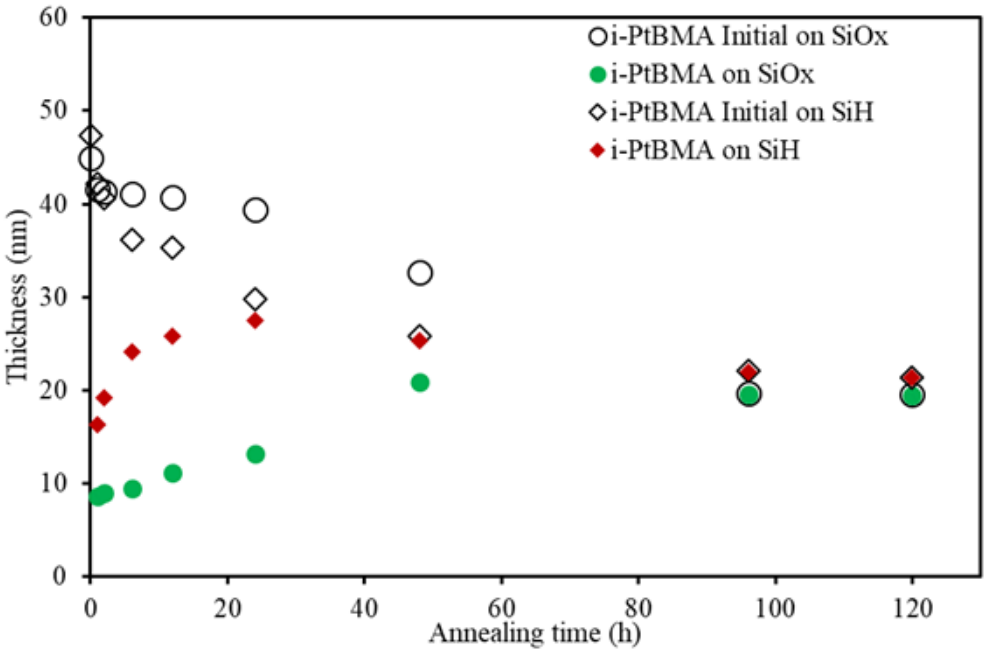

Figure 4.23. Thickness of i-PtBMA layers on SiO_x (circles) and on SiH (diamonds) surfaces before (empty symbols) and after (filled symbols) toluene leaching as a function of annealing time.

Adsorption experiments at 60 °C did not show any difference between a-PtBMA and i-PtBMA even though a-PtBMA was below its T_g. To determine if the tacticity makes any difference the same measurements are repeated using i-PtBMA at 150 °C (T_g + 141 °C). Thicknesses of the i-PtBMA layers before and after leaching on SiH and SiO_x surfaces are plotted as a function of annealing time in Figure 4.23. The initial spun-cast film thicknesses are 47 nm on SiH surface and 45 nm n SiO_x surface. When both samples reached equilibrium, the total film thicknesses were decreased approximately 55%. This is consistent with the thickness reduction in a-PtBMA layers. However, the kinetics of the layer formation after leaching and the reduction in thickness due to thermal annealing are different than those of a-PtBMA. The time to reach equilibrium is 48 h on SiH surface, whereas it takes 96 h to reach equilibrium on SiO_x. Even though i-PtBMA is 141 °C above its T_g, adsorption of chains and the fall of tert-butyl groups are 4 times slower on SiH and 8 times slower on SiO_x compared to the a-PtBMA. It is not just the total time for the reactions but also the shape of the curves on SiO_x is different. During the formation of i-PTBMA layer on SiO_x, there are no maximum observed, instead layers are reaching to their equilibrium structure rather gradually. At the beginning, thickness evolution curve shows a very slow linear growth and then it reaches a plateau value at 20 nm. Similar to a-PtBMA layers the initial thicknesses of presumably adsorbed layers are much thicker than those obtained at 60 °C. Ellipsometry measurements provide the thickness values of the layers when they are forming, however these measurements do not provide information about the composition, chemical and/or surface structure of the layers. It is vital to understand how much of the polymer chains in the layer are adsorbed to the substrate as well as when the layer is composed of crosslinked chains. Answers to these questions are answered partially using ATR-IR and XR measurements and will be discussed later in this section.

PtBMA is not the only polymer we have studied with tert-butyl side group. PneoPMA also has a tert-butyl group and it has quite different adsorption behavior on both surfaces compared to PtBMA due to additional CH_2 moiety in the side group. Earlier adsorption experiments are done at 80 °C (T_g + 50 °C) which is high enough for polymer chains to move around for adsorption and equilibration but not sufficiently

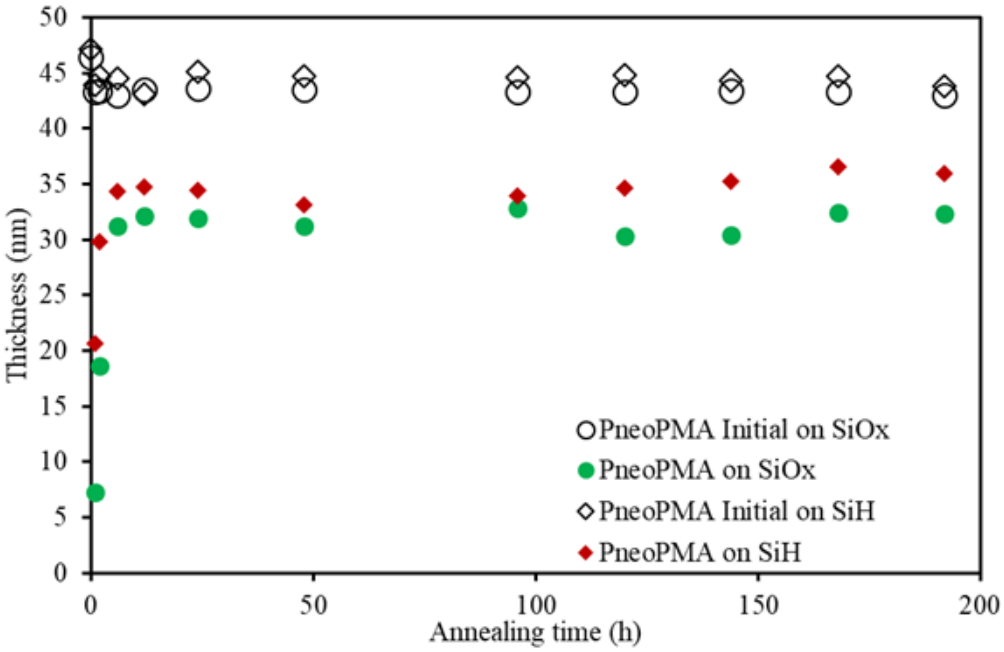

Figure 4.24. Thickness of PneoPMA layers on SiO_x (circles) and on SiH (diamonds) surfaces before (empty symbols) and after (filled symbols) toluene leaching as a function of annealing time.

high to observe a drop of tert-butyl groups. Therefore, the same adsorption experiments are repeated at 150 °C (T_g + 120 °C) to determine the extent of the adsorption vs. chemical reactions if they exist. Thickness values for PneoPMA layers formed at 150 °C on SiO_x and SiH before and after toluene washing are plotted as a function of annealing time in Figure 4.24. Thicknesses of the initial spun-cast layers on SiH and SiO_x are 47 nm. After annealing for various times, thickness values are only reduced around 2 to 3 nm (4 to 6%) which is consistent with the removal of residual solvent. These values imply that the tert-butyl groups are still on the polymer and they are not being removed due to thermal treatment. However, these thickness values alone cannot give information about any other reactions occurring within the film. Even only after 1 h of annealing and toluene leaching, the thicknesses of the presumably adsorbed layers are almost 8 and 21 nm on SiO_x and SiH surfaces, consecutively. There is a very rapid increase at early annealing times and the thickness values reach a plateau value of 34 to 35 nm in 12 h. These thickness values are extremely high for adsorbed layers when the literature and our experience in linear and star polymers taken into

account. The highest normalized adsorbed layer thickness is reported for cyclic PS chains with thickness to radius of gyration ratio (d/R_g) of 2 [45]. If we assume the layers are composed of only adsorbed chains, d/R_g ratio would be equal to 4 in our case. This ratio insinuates that either the chains are stretched in the perpendicular direction similar to polymer brushes or multilayering exist within the film. This adsorption mechanism is ″grafting to″ [46] and it is limited by the diffusion of large polymer chains to the substrate in the presence of already adsorbed chains. ″Grafting to″ method does not produce d/R_g values beyond 2 on flat surfaces. The possibility of multilayering should be investigated in detail in a future work. There is a reason to argue against all the chains in the layer are adsorbed. Adsorption depends highly on the strength of the interaction between polymer segments and the substrate and it is clear from the results presented in Figures 4.6 and 4.18 that adsorbed PneoPMA layer grows much thicker on SiH surface. After 6h annealing, toluene leaching always removes 10 nm from the annealed films. This portion of the film could be non-adsorbed or/and unreacted polymer chains. Obtaining the almost same final layer thickness on both surfaces opposes the view that all the chains are adsorbed. At this point, ATR-IR measurements are necessary to give about the chemical structure of the layer to draw any further information about the possible decomposition reactions.

ATR-IR spectra collected on 47 nm thick spun-cast PneoPMA film on SiO_x surface before annealing and after annealing at 150 °C plus toluene leaching are given in Figure 4.25. After annealing there are no new spectral features appeared and the two spectra are almost identical. This is a clear indication that there were no chemical reactions happened due to annealing at 150 °C. According to literature, lack of β-hydrogens on the PneoPMA leads to decomposition through depolymerization to monomer [44]. However, depolymerization for similar methacrylate based polymers have been observed at and above 200 °C. Very minor reduction in film thickness and no change observed in ATR-IR spectra after annealing convinced us that there are no decomposition reactions happening within the film at 150 °C.

In order to understand the underlying chemical reactions that lead to significant thickness reductions in PtBMA films, ATR-IR measurements are performed both on

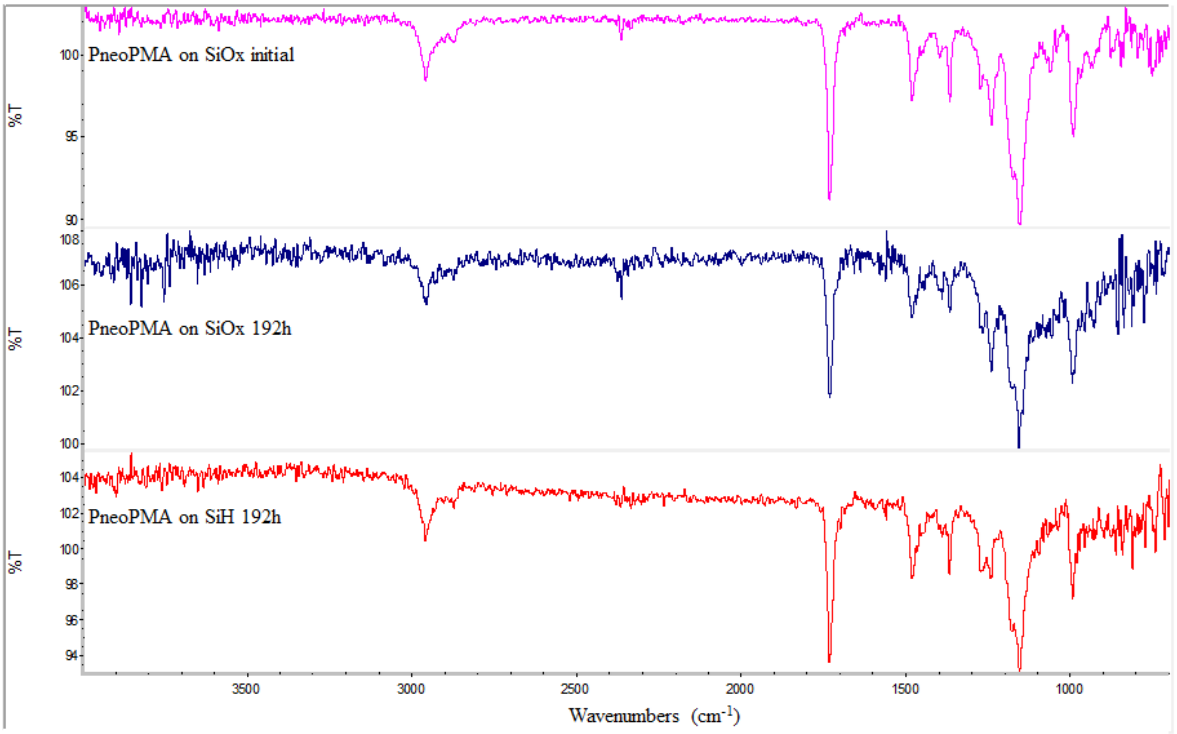

Figure 4.25. ATR-IR spectra for PneoPMA spun-cast layer on SiO_x before annealing (top), PneoPMA on SiO_x after annealing at 150 °C for 192 h (middle), and PneoPMA on SiH after annealing at 150 °C for 192 h (bottom).

i-PtBMA and a-PtBMA layers as a function of annealing time. Since the initial film structure without annealing is same for both a-PtBMA and i-PtBMA on both surfaces we used the ATR-IR spectra of i-PtBMA on SiO_x as the reference and compare it with the spectra obtained after annealing at various times. ATR-IR spectra collected on 47 nm thick spun-cast i-PtBMA film on SiO_x surface before annealing, a-PTBMA layer on SiO_x after annealing at 170 °C for 120 h plus toluene leaching, and a-PTBMA layer on SiH after annealing at 170 °C for 120 h plus toluene leaching are given in Figure 4.26. Initial i-PtBMA film on SiO_x has a peak at 1726 cm^{-1} associated with C=O stretching vibration and a peak at 1146 cm^{-1} for C-O stretching vibration specific for ester structure of PtBMA. Upon completion of the decomposition reactions after 120 h annealing at 170 °C, there are new peaks in the ATR-IR spectra. Carbonyl peak at 1726 cm^{-1} shifts and splits into 2 peaks at 1758 cm^{-1}, 1803 cm^{-1}. Peak for C-O stretching at 1146 cm^{-1} disappeared, and a new peak formed at 1025 cm^{-1}. The position and shape of the new peaks suggested the formation of anhydride within the film. For

non-cyclic anhydrides, high wavenumber C=O symmetric stretching peak is stronger than the lower wavenumber C=O asymmetric stretching peak where as it is vice versa for cyclic anhydrides [47]. Our ATR-IR spectra clearly show that cyclic anhydride is formed in the film after annealing. In fact, there are 2 possible cyclic anhydride structure can be formed during the thermal decomposition of PtBMA depending on the sequence of monomers in the chain. If head-to tail structure is common, then 6-membered glutaric anhydride ring forms between consecutive carboxyl groups and C=O peaks appear at 1802 and 1756 cm^{-1} in the IR spectrum. When head-to-head or tail-to-tail sequence is present then 5-membered succinic anhydride ring forms with associated C=O stretching peaks at higher wavenumbers of 1855 and 1776 cm^{-1} due to higher ring strain. We have concluded that our layer after 120 h annealing is mainly composed of glutaric anhydride. The first step for the formation of glutaric anhydride from tert-butyl methacrylate is the formation of carboxylic acid and it is puzzling that we do not observe neither OH stretchings nor C=O peak associated with the carboxylic acid formation.

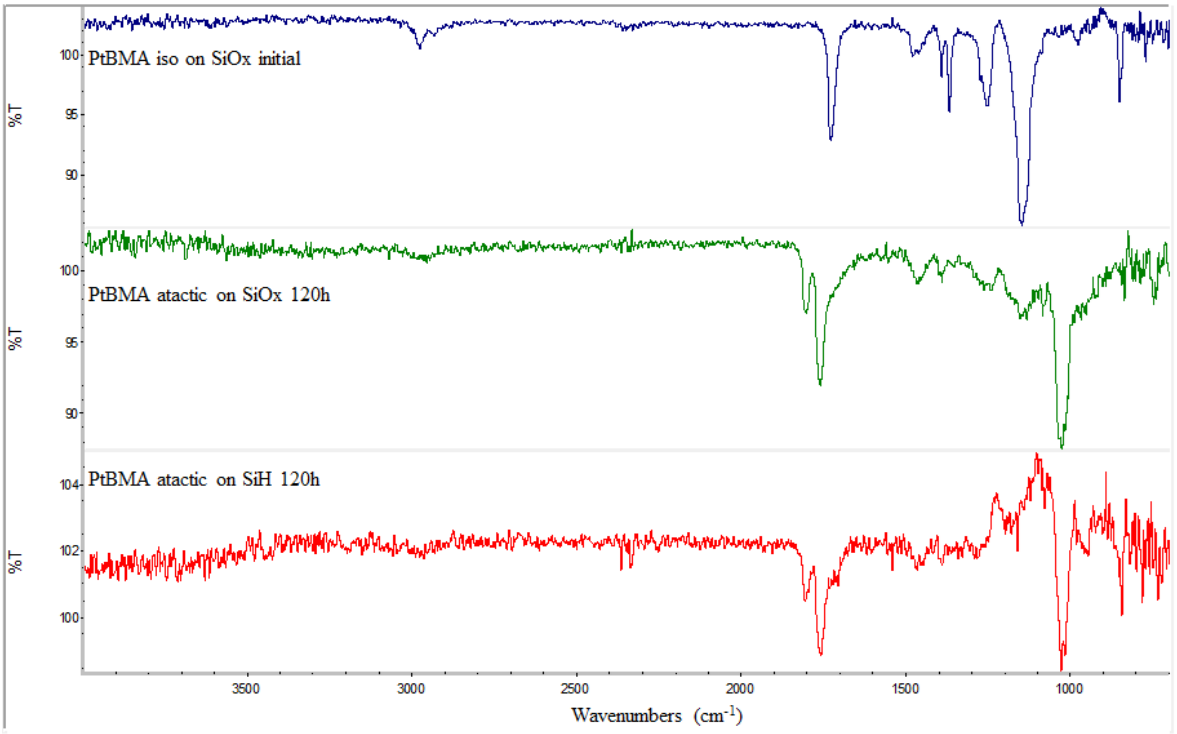

Figure 4.26. ATR-IR spectra for i-PtBMA spun-cast layer on SiO_x before annealing (top), a-PtBMA on SiO_x after annealing at 170 °C for 120 h (middle), and a-PtBMA on SiH after annealing at 170 °C for 120 h (bottom).

Ellipsometry measurements indicated that the equilibrium layer thicknesses for a-PtBMA and i-PtBMA are similar but their reaction kinetics are different. We have repeated the ATR-IR measurements on i-PtBMA layers in the same way for a-PtBMA. ATR-IR spectra collected on 47 nm thick spun-cast i-PtBMA film on SiO_x surface before annealing, i-PTBMA layer on SiO_x after annealing at 150 °C for 120 h plus toluene leaching, and i-PTBMA layer on SiH after annealing at 150 °C for 120 h plus toluene leaching are given in Figure 4.27. Based on the same peak shifts observed for a-PtBMA layers after annealing, we have confirmed the same cyclic glutaric anhydride structure for i-PtBMA layers. However, the peaks observed for initial film at 1720 cm^{-1} associated with symmetric stretching of C=O group, and C-O peak at 1130 cm^{-1} did not completely disappear. These results suggest that reaction is not completed at 150 °C upon 120 h annealing for i-PtBMA film.

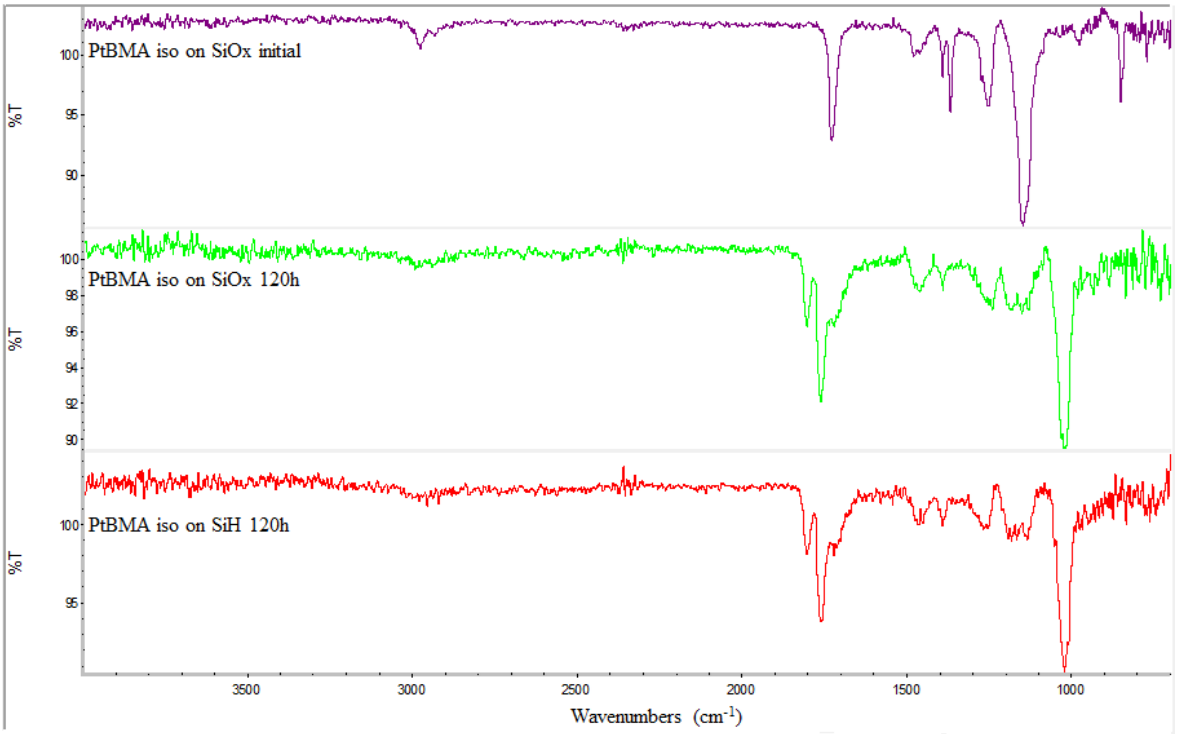

Figure 4.27. ATR-IR spectra for i-PtBMA spun-cast layer on SiO_x before annealing (top), i-PtBMA on SiO_x after annealing at 150 °C for 120 h (middle), and i-PtBMA on SiH after annealing at 150 °C for 120 h (bottom).

Once we established the chemical structure of the i-PtBMA film for the spun-cast layer and the final sample after 120 h annealing at 150 °C, ATR-IR spectra collected for all the annealing times in between and the results are plotted in Figure 4.28. These plots show us the evolution of the reaction as a function of annealing time. There are no changes in the collected ATR-IR spectra up to 48 h of annealing. Spectra for 48 h of annealing have hints of changes at the C=O peak position. Even though original peak is present there are two more peaks forming at the wavenumbers associated with cyclic glutaric anhydride. These peaks become stronger and the original peak becomes weaker at 96 h of annealing. We have already determined from the evolution of thickness that the reaction is very slow compared to a-PtBMA on SiO_x surface. The slope of the thickness increase is changed at 48 h and ATR-IR measurements indicate that the glutaric anhydride starts forming at 48 h. Since prerequisite for the existence of cylic glutaric anhydrides is the formation of polymethacrylic acid from PtBMA,

we speculate that the de-esterification finished before 48 h. Unfortunately, we cannot prove the formation of the carboxylic acids due to lack of broad peak between 2500 and 3500 cm^{-1} associated with OH stretchings and C=O peak at 1698 cm^{-1}. When the same experiment is performed on SiH surface, we have seen that the reaction proceeded faster based on the ellipsometry measurements. ATR-IR spectra are measured for i-PtBMA adsorption at 150 °C for various annealing times and the results are plotted in Figure 4.29. The only difference between these two experiments is the enthalpic interactions between the polymer segments and the substrate surface. Earlier we have determined that the enthalpic interactions are stronger between PtBMA and SiH surface compared to SiO_x surface independent of tacticity. Anhydride peaks appear in the ATR-IR spectrum at 6 h annealing on SiH surface. This is also consistent with the ellipsometry results. Then original carbonyl peak disappears and double peaks associated with carbonyl stretching of glutaric anhydride becomes stronger on both surfaces, the formation of cyclic glutaric anhydride starts after the adsorbed layer reached its equilibirum thickness. This data suggest surface energy plays an important role in reaction kinetic. Since adsorption reached to equilibrium faster on SiH surface, reaction starts earlier as well compared to SiO_x surface.

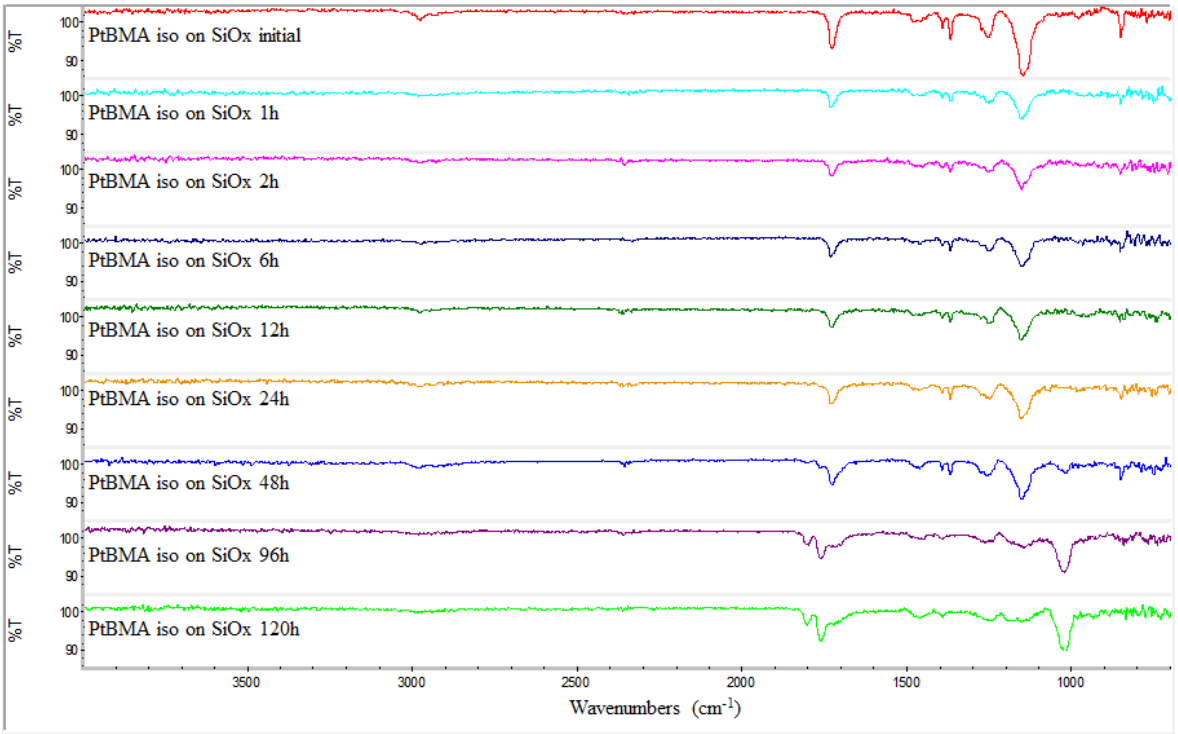

Figure 4.28. ATR-IR spectra for i-PtBMA layers on SiO_x surface collected after various annealing times at 150 °C. Annealing times are specified in each plot.

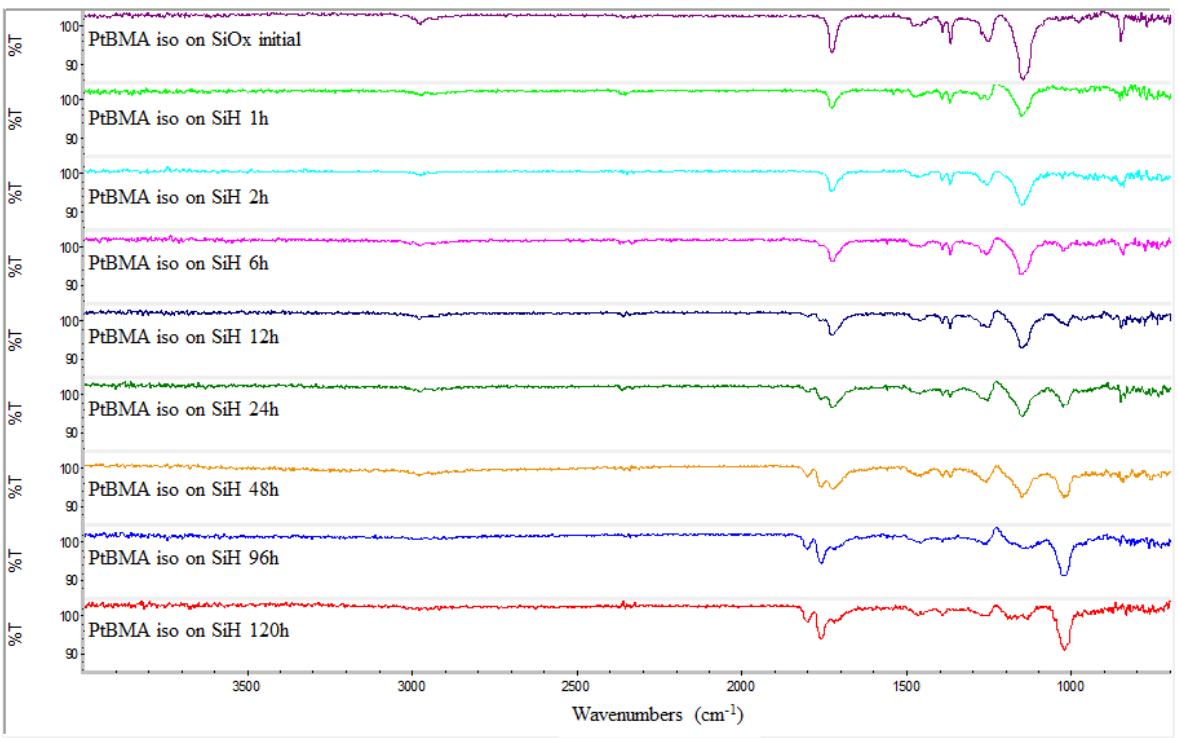

Figure 4.29. ATR-IR spectra for i-PtBMA layers on SiH surface collected after various annealing times at 150 °C. Annealing times are specified in each plot.

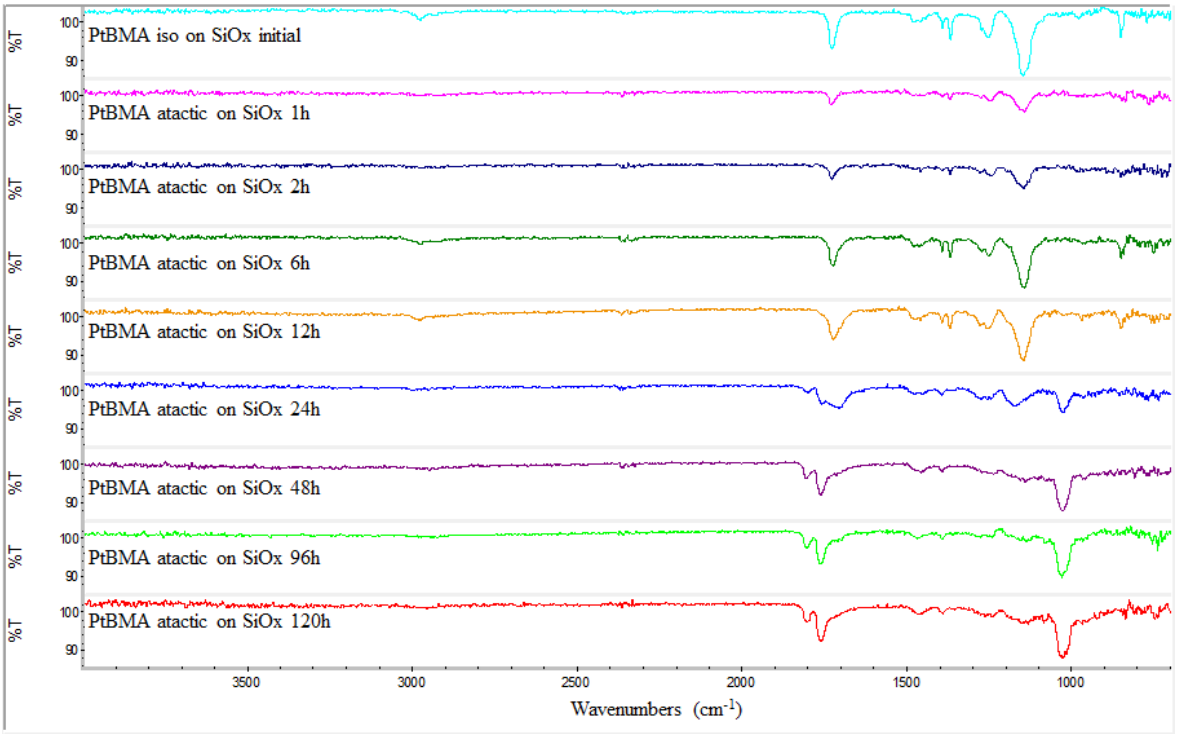

Figure 4.30. ATR-IR spectra for a-PtBMA layers on SiO_x surface collected after various annealing times at 150 °C. Annealing times are specified in each plot.

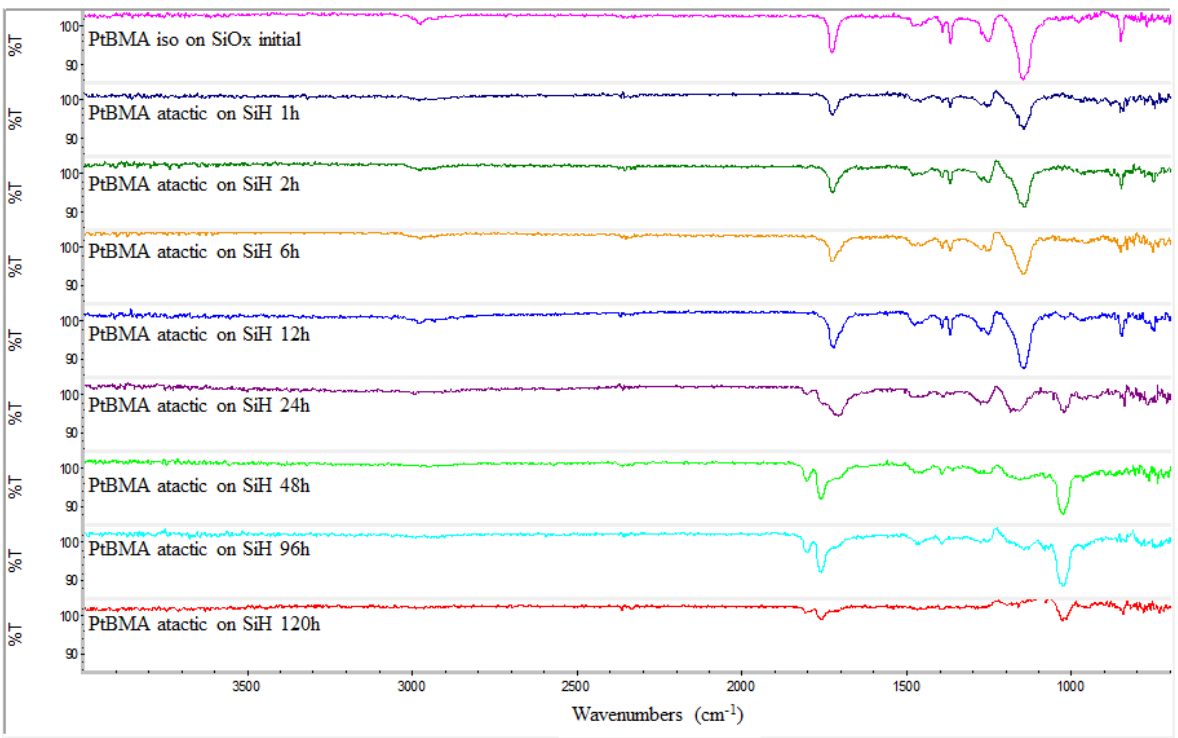

Figure 4.31. ATR-IR spectra for a-PtBMA layers on SiH surface collected after various annealing times at 150 °C. Annealing times are specified in each plot.

ATR-IR spectra measured for a-PtBMA on SiO_x and on SiH for various annealing times at 170 °C are shown in Figures 4.30 and 4.31, consecutively. Consistent with ellipsometry measurements the cyclic glutaric anhydride starts forming within the film at 24 h on both surfaces. This reaction temperature is only 50 °C above the $T_{g,bulk}$ for a-PtBMA whereas the reaction temperature is 141 °C above the $T_{g,bulk}$ for i-PtBMA. This is an important difference that explains why reaction proceed slower on SiH surface for a-PtBMA. Another interesting observation is that the surface energy of the substrate did not change the reaction kinetics for atactic polymer. Especially, this equal affinity of a-PtBMA at 170 °C to both substrates implies that the strength of the interactions depends on the temperature. This will be an important question for future work.

4.4. XR Results for the Layers in the Presence of Decomposition Reactions

After revealing chemical structure and the layer thicknesses as a function of annealing time, we investigated the detailed structure of layers formed through adsorption followed by decomposition reactions. Layer structure is determined in the perpendicular direction using XR measurements on the equilibrated films after toluene leaching.

4.4.1. i-PtBMA Reaction on Hydrophilic and Hydrophobic Surfaces

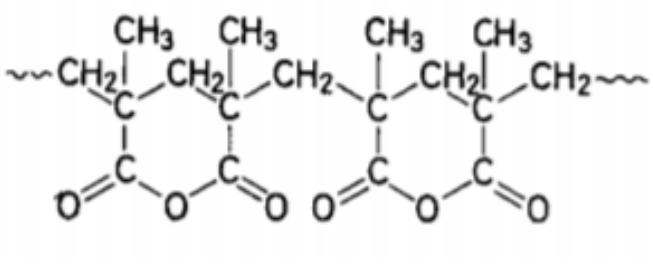

Figure 4.32. Chemical structure of poly(glutaric anhydride) unit.

IR measurements demonstrated that even though we have started with a-PtBMA or i-PtBMA, at the end of the reaction we had poly(glutaric anhydride) (PGA) (Figure 4.32). When the amount of PGA in the film increases, the chains become more hydro-

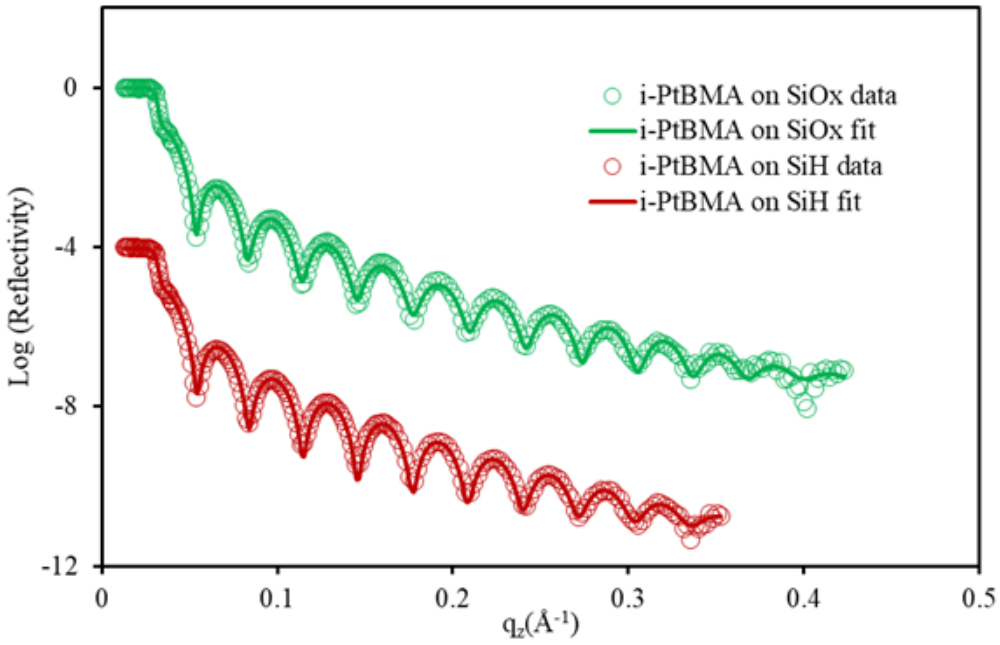

Figure 4.33. Logarithm of reflectivity as a function of q_z for 120 h annealed i-PtBMA on SiO_x (green circles) and on Si-H (red circles). Curve for SiH surface has been shifted vertically by log $(10)^{-4}$ for clarity.

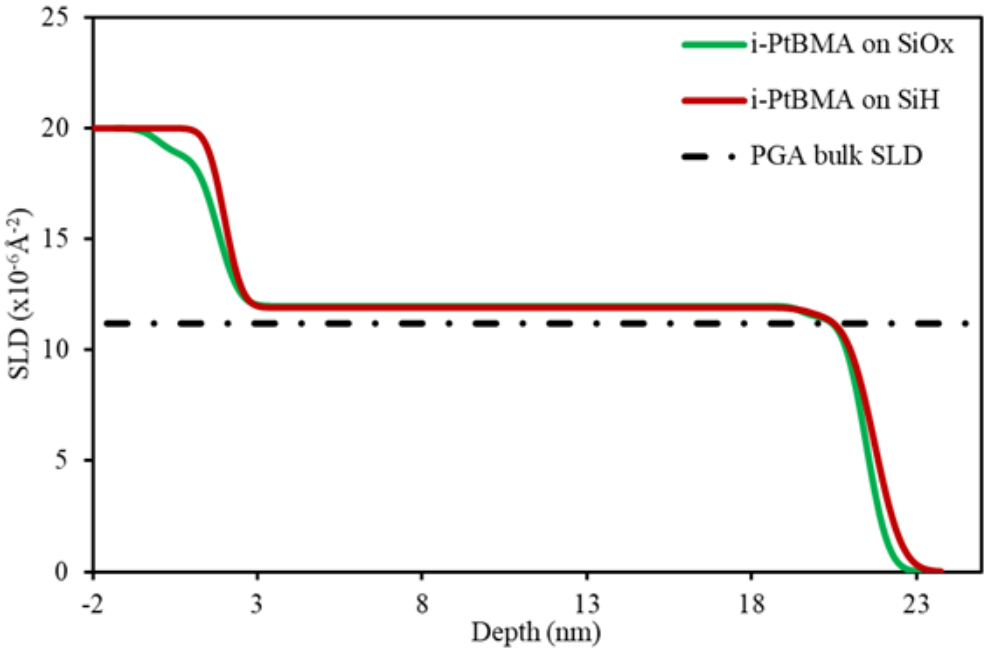

Figure 4.34. Scattering length density (SLD) as a function of depth for 120 h annealed i-PtBMA at 150 °C on SiO_x (green) and on SiH (red).

philic on one side and backbone keeps the initial hydrophobicity. This produces thicker layers on both surfaces compared to earlier adsorption experiments at lower annealing temperatures. XR curves for 120 h annealed i-PtBMA at 150 °C followed by toluene leaching are shown in Figure 4.33. It is obvious from the presence of multiple Kiessig fringes that the layers are thick. The best fit lines obtained from bilayer model are also shown in Figure 4.34 and there is a very good agreement between experimental data and the bilayer model. The XR SLD profiles derived from the bilayer model fitting are shown in Figure 4.34. SLD profiles are identical to each other on these two different surfaces. On both surfaces, the layer next to the substrate is 17.7 nm thick with SLD value of 1.19 x 10^{-5} Å^{-2} which is slightly above bulk SLD of PGA. Second layer has 2 nm thickness with SLD value of 1.15 x 10^{-5} Å^{-2} which is almost bulk SLD of PGA. Total thickness of the layers are in excellent agreement with the thicknesses obtained by ellipsometry. Both layers have very smooth air surfaces. Very thin layers at the top surface with slightly lower SLD values may suggest a slightly different structure but we did not want to draw too much attention since the SLD difference between the layers is so small.

4.4.2. a-PtBMA Reaction on Hydrophilic and Hydrophobic Surfaces

XR curves are given for 120 h annealed a-PtBMA at 170 °C on SiO_x and SiH surfaces in Figure 4.35 along with the best fits. SLD profiles as a function of depth are given in Figure 4.36. XR curves are fit using a single layer model of uniform density throughout the film. This is different than the i-PtBMA results where we have observed a 2 nm thick layer with a slightly lower SLD on the air surface. Even though this difference is very small, it may still indicate that in i-PtBMA case, the reaction may not be completed at the surface. On SiO_x surface, the SLD value of the 21.2 nm thick layer is 1.13 x 10^{-5} Å^{-2} which is nearly equal to bulk SLD of PGA. On SiH surface, it has 22.3 nm thickness with SLD value of 1.05 x 10^{-5} Å^{-2} which is slightly below the bulk SLD of PGA. The PGA layer formed from a-PtBMA on the SiO_x surface is rougher than on SiH surface.

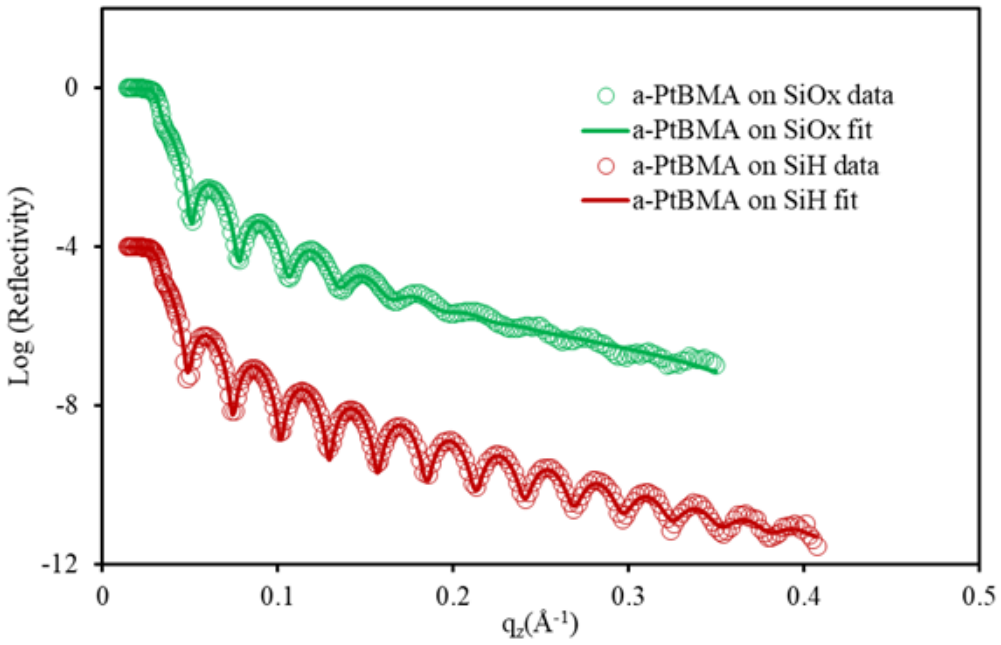

Figure 4.35. Logarithm of reflectivity as a function of q_z for 120 h annealed a-PtBMA on SiO_x (green circles) and on Si-H (red circles). Curve for SiH surface has been shifted vertically by log $(10)^{-4}$ for clarity.

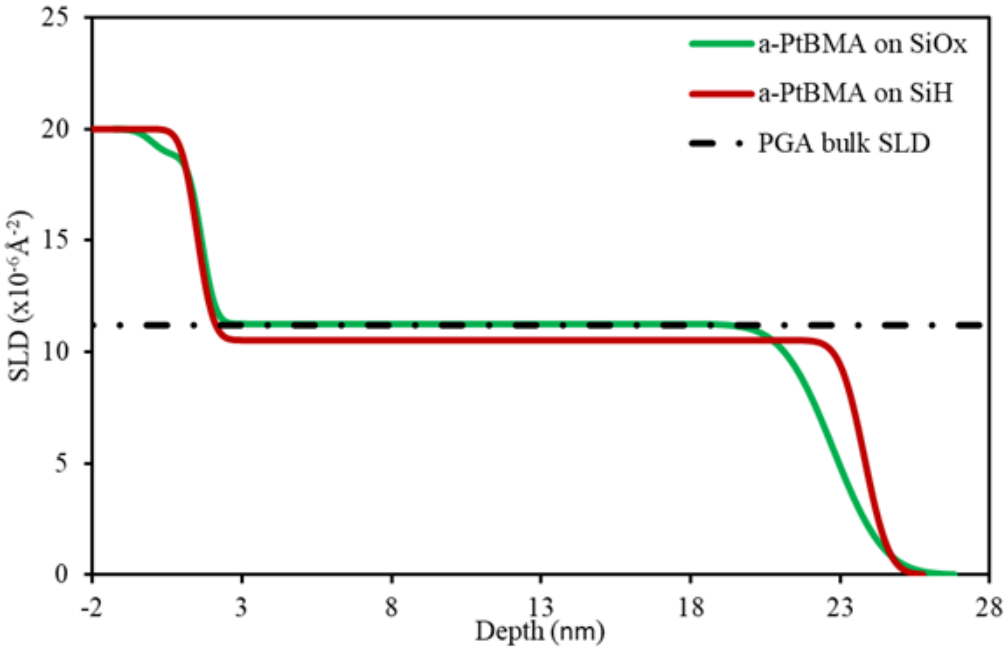

Figure 4.36. Scattering length density (SLD) as a function of depth for 120 h annealed a-PtBMA at 170 °C on SiO_x (green) and on SiH (red).

4.4.3. PneoPMA Reaction on Hydrophilic and Hydrophobic Surfaces

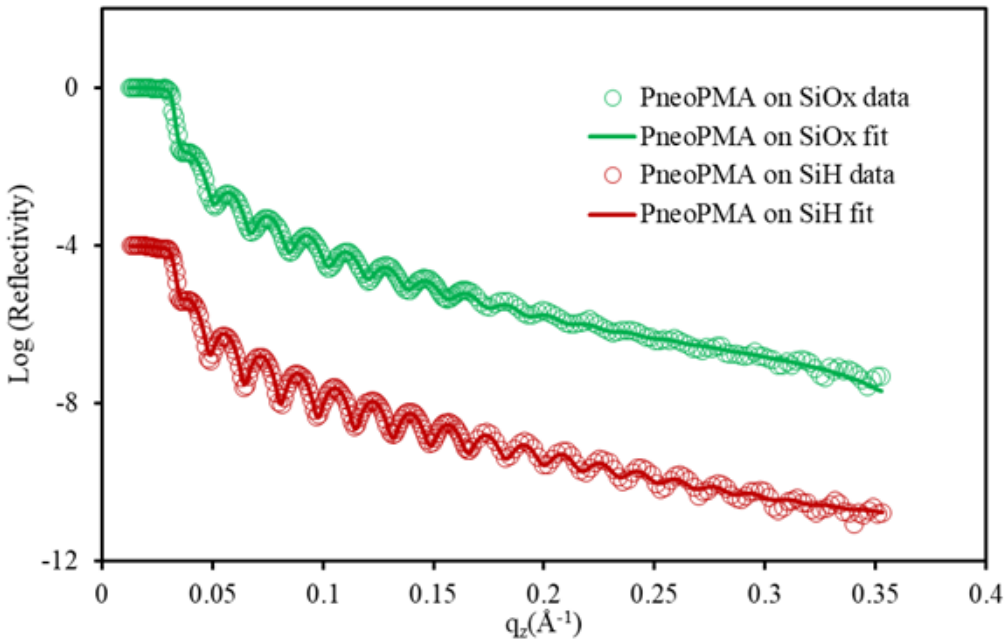

Figure 4.37. Logarithm of reflectivity as a function of q_z for 120 h annealed PneoPMA on SiO_x (green circles) and on Si-H (red circles). Curve for SiH surface has been shifted vertically by log $(10)^{-4}$ for clarity.

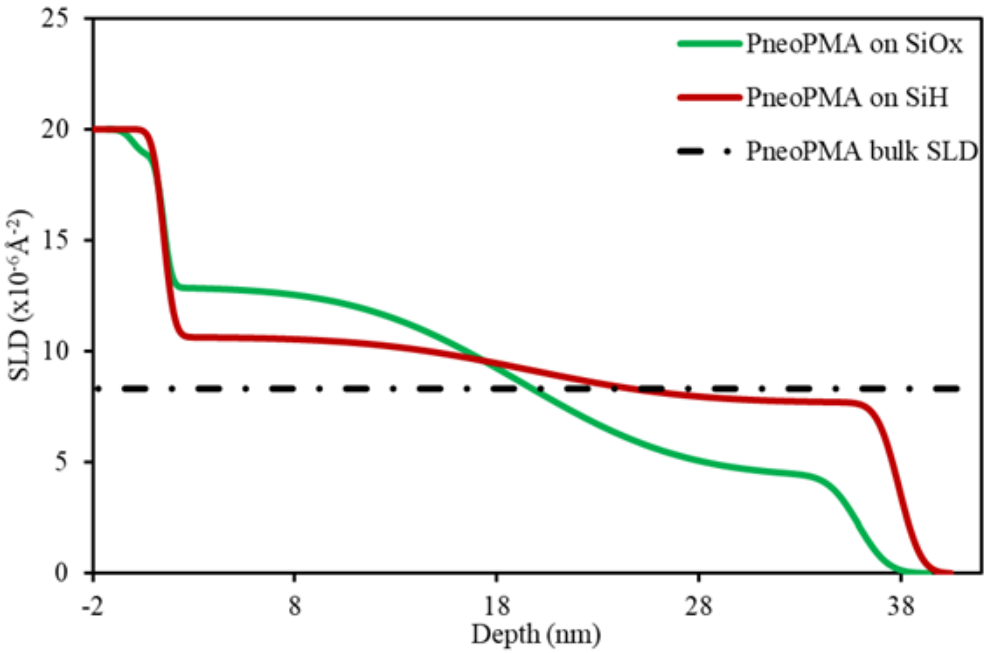

Figure 4.38. Scattering length density (SLD) as a function of depth for 120 h annealed PneoPMA at 150 °C on SiO_x (green) and on SiH (red).

Ellipsometry and ATR-IR measurements did not provide any clues for decomposition reactions during the annealing of PneoPMA at 150 °C. XR measurements for PneoPMA layers on SiO_x and SiH surfaces are shown in Figure 4.37 and SLD profiles obtained from the best fits are plotted in Figure 4.38. XR experimental curves are best fit using bilayer models. On SiO_x surface, the bottom layer is 17.8 nm thick with SLD value of 1.29 x 10^{-5} $Å^{-2}$ which is 40% above its bulk SLD value. Second layer has 16.54 nm thickness with 4.34 x 10^{-6} $Å^{-2}$ which is way below its bulk SLD value. This very low value indicates that the second layer is not a complete smooth layer, instead it is a patchy layer with a few chains sticking out but mostly air in between these chains. On SiH surface, bottom layer has 18.1 nm thickness with SLD value of 1.06 x 10^{-5} $Å^{-2}$ which is slightly above its bulk SLD value, and the top layer has 18.3 nm thickness with SLD value of 7.69 x 10^{-6} $Å^{-2}$ which is below its bulk SLD value. The top layer is not a complete layer but this time the fraction of PneoPMA chains in the layer is larger than that on SiO_x surface. There is also a broad transition between the layers.

5. CONCLUSION

The most significant result of this work is that the thickness and the structure of adsorbed polymer layers are dramatically influenced by the length and stiffness of the side chains. For side chains that contain normal alkane groups, as the alkyl unit number increases the adsorbed layer thickness decreases on both hydrophobic and hydrophilic surfaces. Although, introduction of bulky and stiff side chains tends to maximize the adsorbed layer thickness on either of the surfaces the clear correlation still needs to be resolved in detail. Being able to control the character of the adsorbed layer with only minor changes in the side chain chemistry without any change in the backbone offers new pathways to tune the physical properties of thin polymer films.

Time dependent ellipsometry measurements and XR measurements on the equilibrated layers demonstrated that increasing length of n-alkanes in side chain for methacrylate based polymers give rise to a decrease in adsorbed layer thickness on both hydrophobic and hydrophilic surfaces. However, the magnitude of the decrease was much more prominent on the hydrophilic surface most likely due to loss of hydrogen bonding ability of the segments with the underlying substrate. On the contrary, it is quite surprising that the layer thickness decreases on the hydrophobic substrate when the hydrophobicity of the overall chain increases. These observations imply that the side chains composed of normal alkanes are effectively blocking the segment-substrate interactions to inhibit the formation of adsorbed layers. At equilibrium, the structure of adsorbed methacrylate based polymer layers are approximated by a single layer of uniform mass density on SiH and a bilayer with a higher density layer next to the substrate on SiO_x surface. Overall, the mass density of the layers on SiH surface was slightly higher than the mass density of the corresponding polymers in bulk. For PiBoMA, the difference between the mass density of the layer and the bulk was 25% even though at the annealing temperature (T_g - 20 °C). Although, it did not reach equilibrium, adsorbed PiBoMA layer is the thickest adsorbed layer on SiO_x surface. Isobornyl group is the stiffest side group used in this study. Tertiary butyl and neopentyl groups yield also thick layers on SiH surface but the layer thicknesses are flummoxing on SiO_x

surface. Adsorbed layer thicknesses of i-PtBMA and a-PtBMA are almost negligible on SiO_x surface whereas PneoPMA formed an appreciably thick adsorbed layer on SiO_x surface. The difference between the chemical structures of these two polymers is a single CH_2 unit between the oxygen and the bulky tertiary butyl groups. Addition of this CH_2 group seems to change the conformation of the polymer around the substrate in such a way that the oxygen and the carbonyl oxygen is able to make hydrogen bonding with the hydroxyl functionalities on SiO_x surface. The same explanation is also true for PiBoMA adsorption on SiO_x. Unfortunately, it is not possible to detect the orientation of the side groups at a buried interface with XR or ellipsometry measurements. It can be done using sum frequency generation technique, but this topic is left as a future work.

Adsorption measurements using i-PtBMA and a-PtBMA at 60 °C were almost identical which may imply that tacticity does not play any role on the adsorption. At this point we cannot draw much attention to this result since 60 °C is T_g + 50 °C for i-PtBMA but it is 58 °C below $T_{g,bulk}$ of a-PtBMA. It was not possible to make a direct comparison because at T_g + 50 °C for a-PtBMA, both polymers have side reactions triggered by the drop of tert-butyl groups. Decoupling adsorption from proceeding side reactions at late stages is impossible. However, at early annealing times where the shape of thickness evolution curves indicate that the adsorption is dominant process, one can infer tacticity has an effect on the kinetics. On SiO_x surface, i-PtBMA layer forms much slower with a gradual linear increase. The fact that i-PtBMA is annealed at T_g + 141 °C clearly suggests that the adsorption is slower for isotactic polymer.

Decomposition of a-PtBMA at T_g + 50 °C and i-PtBMA at T_g + 141 °C is monitored as a function of annealing time. In both cases, we do not observe decomposition to monomer through thermolysis. Instead, as suggested in the literature, PtBMA, through de-esterification, is converted to first poly(methacrylic acid) and then to anhydride [48]. Frequencies of the carbonyl peaks in ATR-IR measurements indicated that the final layer is composed of glutaric anhydride. Tacticity did not play any role on the final structure but as emphasized earlier it has influenced the reaction kinetics. Adsorption experiments for PneoPMA at T_g + 120 °C did not cause any decompo-

sition based on lack of significant changes in total film thickness after annealing and unchanged ATR-IR spectra before and after annealing. Novakovic et al. suggested that the main degradation route for PneoPMA is the decomposition to monomer since there are no β-hydrogens [44]. However, the temperature we have used in the experiment is not high enough to cause any decomposition to monomer. As far as we know PneoPMA at T_g + 120 °C yield the thickest adsorbed layers measured. When the thickness of the adsorbed PneoPMA layer is normalized with its R_g value, we obtain d/R_g value of 4. This value indicates either chains are stretched in the perpendicular direction or there are multilayers of PneoPMA.

REFERENCES

1. Decher, G., "Fuzzy nanoassemblies: Toward layered polymeric multicomposites", *Science*, Vol. 277, No. 5330, pp. 1232–1237, 1997.

2. Peyratout, C. S. and L. Dähne, "Tailor-made polyelectrolyte microcapsules: From multilayers to smart containers", *Angewandte Chemie - International Edition*, Vol. 43, No. 29, pp. 3762–3783, 2004.

3. Arumugam, S., S. V. Orski, J. Locklin and V. V. Popik, "Photoreactive Polymer Brushes for High-Density Patterned Surface Derivatization Using a Diels− Alder Photoclick Reaction", *J.Am.Chem.Soc.*, Vol. 134, pp. 179–182, 2012.

4. Zhao, C., L.-Y. Li, M.-M. Guo and J. Zheng, "Functional polymer thin films designed for antifouling materials and biosensors", *Chemical Papers*, Vol. 66, No. 5, pp. 323–339, 2012.

5. Housmans, C., M. Sferrazza and S. Napolitano, "Kinetics of irreversible chain adsorption", *Macromolecules*, Vol. 47, No. 10, pp. 3390–3393, 2014.

6. Kallrot, N., *Dynamics of Polymer Adsorption onto Solid Surfaces in Good Solvent*, Ph.D. Thesis, Lund University, 2016.

7. Silberberg, A., "Adsorption of flexible macromolecules. IV. Effect of solvent-solute interactions, solute concentration, and molecular weight", *The Journal of Chemical Physics*, Vol. 48, No. 7, pp. 2835–2851, 1968.

8. Hoeve, C. A. J., "On the general theory of polymer absorption at a surface", *Journal of Polymer Science Part C: Polymer Symposia*, Vol. 30, No. 1, pp. 361–367, 3 2007.

9. Scheutjens, J. M. and G. J. Fleer, "Statistical theory of the adsorption of inter-

acting chain molecules. 1. Partition function, segment density distribution, and adsorption isotherms", *Journal of Physical Chemistry*, Vol. 83, No. 12, pp. 1619–1635, 1979.

10. Manciu, M. and E. Ruckenstein, "Loops, tails and trains: A simple model for structural transformations of grafted adsorbing neutral polymer brushes", *Journal of Colloid and Interface Science*, Vol. 354, No. 1, pp. 61–69, 2011.

11. Guiselin, O., "Irreversible adsorption of a concentrated polymer solution", *Europhysics Letters*, Vol. 17, No. 3, pp. 225–230, 1992.

12. Jiang, N., J. Shang, X. Di, M. K. Endoh and T. Koga, "Formation mechanism of high-density, flattened polymer nanolayers adsorbed on planar solids", *Macromolecules*, Vol. 47, No. 8, pp. 2682–2689, 2014.

13. Gin, P., N. Jiang, C. Liang, T. Taniguchi, B. Akgun, S. K. Satija, M. K. Endoh and T. Koga, "Revealed architectures of adsorbed polymer chains at solid-polymer melt interfaces", *Physical Review Letters*, Vol. 109, No. 26, pp. 1–5, 2012.

14. Durning, C. J., B. O'Shaughnessy, U. Sawhney, D. Nguyen, J. Majewski and G. S. Smith, "Adsorption of poly(methyl methacrylate) melts on quartz", *Macromolecules*, Vol. 32, No. 20, pp. 6772–6781, 1999.

15. Burroughs, M. J., S. Napolitano, D. Cangialosi and R. D. Priestley, "Direct measurement of glass transition temperature in exposed and buried adsorbed polymer nanolayers", *Macromolecules*, Vol. 49, No. 12, pp. 4647–4655, 2016.

16. Koga, T., N. Jiang, P. Gin, M. K. Endoh, S. Narayanan, L. B. Lurio and S. K. Sinha, "Impact of an irreversibly adsorbed layer on local viscosity of nanoconfined polymer melts", *Physical Review Letters*, Vol. 107, No. 22, pp. 1–5, 2011.

17. Martínez-Tong, D. E., B. Vanroy, M. Wübbenhorst, A. Nogales and S. Napolitano, "Crystallization of poly(l-lactide) confined in ultrathin films: Competition between

finite size effects and irreversible chain adsorption", *Macromolecules*, Vol. 47, No. 7, pp. 2354–2360, 2014.

18. Wang, S. F., Z. Jiang, S. Narayanan and M. D. Foster, "Dynamics of surface fluctuations on macrocyclic melts", *Macromolecules*, Vol. 45, No. 15, pp. 6210–6219, 2012.

19. Jiang, N., L. Sendogdular, X. Di, M. Sen, P. Gin, M. K. Endoh, T. Koga, B. Akgun, M. Dimitriou and S. Satija, "Effect of CO2 on a mobility gradient of polymer chains near an impenetrable solid", *Macromolecules*, Vol. 48, No. 6, pp. 1795–1803, 2015.

20. Davis, M. J., B. Zuo and R. D. Priestley, "Competing polymer-substrate interactions mitigate random copolymer adsorption", *Soft Matter*, Vol. 14, No. 35, pp. 7204–7213, 9 2018.

21. Keddie, J. L., R. A. Jones and R. A. Cory, "Interface and surface effects on the glass-transition temperature in thin polymer films", *Faraday Discussions*, Vol. 98, pp. 219–230, 1994.

22. Priestley, R. D., M. K. Mundra, N. J. Barnett, L. J. Broadbelt and J. M. Torkelson, "Effects of Nanoscale Confinement and Interfaces on the Glass Transition Temperatures of a Series of Poly(n-methacrylate) Films", *Australian Journal of Chemistry*, Vol. 60, No. 10, p. 765, 2007.

23. Ellison, C. J. and J. M. Torkelson, "The distribution of glass-transition temperatures in nanoscopically confined glass formers", *Nature Materials*, Vol. 2, No. 10, pp. 695–700, 2003.

24. Roth, C. B., K. L. McNerny, W. F. Jager and J. M. Torkelson, "Eliminating the enhanced mobility at the free surface of polystyrene: Fluorescence studies of the glass transition temperature in thin bilayer films of immiscible polymers", *Macromolecules*, Vol. 40, No. 7, pp. 2568–2574, 4 2007.

25. Napolitano, S., A. Pilleri, P. Rolla and M. Wübbenhorst, "Unusual deviations from bulk behavior in ultrathin films of poly(tert-butylstyrene): Can dead layers induce a reduction of Tg?", *ACS Nano*, Vol. 4, No. 2, pp. 841–848, 2010.

26. Grohens, Y., M. Brogly, C. Labbe, M.-O. David and S. Jacques, "Poly (methyl methacrylate) at Interfaces", *Langmuir*, Vol. 14, No. 11, pp. 2929–32, 1998.

27. Maas, J. H., M. A. Cohen Stuart, F. A. Leermakers and N. A. Besseling, "Wetting transition in a polymer brush: Polymer droplet coexisting with two film thicknesses", *Langmuir*, Vol. 16, No. 7, pp. 3478–3481, 2000.

28. Tang, T., A. Jagota, M. K. Chaudhury and C. Y. Hui, "Thermal fluctuations limit the adhesive strength of compliant solids", *Journal of Adhesion*, Vol. 82, No. 7, pp. 671–696, 2006.

29. Kim, H., A. Rühm, L. B. Lurio, J. K. Basu, J. Lal, D. Lumma, S. G. Mochrie and S. K. Sinha, "Surface Dynamics of Polymer Films", *Physical Review Letters*, Vol. 90, No. 6, p. 4, 2003.

30. Zhou, Y., Q. He, F. Zhang, F. Yang, S. Narayanan, G. Yuan, A. Dhinojwala and M. D. Foster, "Modifying Surface Fluctuations of Polymer Melt Films with Substrate Modification", *ACS Macro Letters*, Vol. 6, No. 9, pp. 915–919, 2017.

31. Damme, H., A. Hogt and J. Feijen, "Surface Mobility and Structural Transitions of Poly (n-alkyl methacrylates) Probed by Dynamic Contact Angle Measurements", *Journal of Colloid and Interface Sience*, Vol. 114, No. 1, pp. 167–172, 1986.

32. Mortazavian, H., C. J. Fennell and F. D. Blum, "Surface Bonding Is Stronger for Poly(methyl methacrylate) than for Poly(vinyl acetate)", *Macromolecules*, Vol. 49, No. 11, pp. 4211–4219, 2016.

33. Hogt, A. H., D. E. Gregonis, I. J. D. Andrade, S. W. Kim, J. Dankert and J. Feijen, "Wettability and Zeta Potentials of a Series of Methacrylate Polymers and

Copolymers", *Journal of Colloid and Interface Sience*, Vol. 106, No. 2, 1985.

34. R. Vig, J. and J. W. Le bus, "UV / Ozone of Surfaces", *IEEE Transactions on Parts, Hybrids, and Packaging*, Vol. PHP-12, No. 4, pp. 365–370, 1976.

35. Cristóvão, R., C. Botelho, R. Martins and R. Boaventura, "Pollution prevention and wastewater treatment in fish canning industries of Northern Portugal", *International Proceedings of Chemical, Biological and Environmental Engineering*, Vol. 32, No. 1, pp. 12–16, 2012.

36. Bellenger, V., J. Kaltenecker-Commerçon, J. Verdu and P. Tordjeman, "Interactions of solvents with poly(methyl methacrylate)", *Polymer*, Vol. 38, No. 16, pp. 4175–4184, 1997.

37. Sahu, N., B. Parija and S. Panigrahi, "Fundamental understanding and modeling of spin coating process: A review", *Indian Journal of Physics*, Vol. 83, No. 4, pp. 493–502, 2009.

38. Meyerhofer, D., "Characteristics of resist films produced by spinning", *Journal of Applied Physics*, Vol. 49, No. 7, pp. 3993–3997, 1978.

39. Mccrackin, F., E. Passaglia, R. Stromberg and H. Steinberg, "Measurement of the Thickness and Refractive Index of Very Thin Films 1 and the Optical Properties of Surfaces by Ellipsometry", *Journal of Research of the National Bureau of Standards*, Vol. 67, No. 4, 1963.

40. Ciccariello, S., J. Goodisman and H. Brumberger, "On the porod law", *Journal of Applied Crystallography*, Vol. 21, pp. 117–128, 1988.

41. Huang, T. C., R. Gilles and G. Will, "Thin-film thickness and density determination from x-ray reflectivity data using a conventional power diffractometer", *Thin Solid Films*, Vol. 230, No. 2, pp. 99–101, 1993.

42. Özer S., *Adsorption of Branched Polymer Chains onto Solid Substrates*, Ph.D. Thesis, Bogazici University, 2019.

43. Treat, N. D., N. Ayres, S. G. Boyes and W. J. Brittain, "A facile route to poly(acrylic acid) brushes using atom transfer radical polymerization", *Macromolecules*, Vol. 39, No. 1, pp. 26–29, 2006.

44. Novaković, K., L. Katsikas and I. G. Popović, "The thermal degradation of poly(iso-butyl methacrylate) and poly(sec-butyl methacrylate)", *Journal of the Serbian Chemical Society*, Vol. 65, No. 12, pp. 867–875, 2000.

45. He, Q., S. Narayanan, D. T. Wu and M. D. Foster, "Confinement Effects with Molten Thin Cyclic Polystyrene Films", *ACS Macro Letters*, Vol. 5, No. 9, pp. 999–1003, 9 2016.

46. Boyes, S. G., A. M. Granville, M. Baum, B. Akgun, B. K. Mirous and W. J. Brittain, "Polymer brushes - Surface immobilized polymers", *Surface Science*, Vol. 570, No. 1-2, pp. 1–12, 10 2004.

47. Smith, B. C., "The C=O Bond, Part IV: Acid Anhydrides", *Spectroscopy*, Vol. 33, No. 3, pp. 16–20, 2018.

48. Grant, D. H. and N. Grassie, "The thermal decomposition of polymethacrylic acid", *Polymer*, Vol. 1, No. C, pp. 125–134, 1960.